Ore Geology Reviews 130 (2021) 103945

Contents lists available at ScienceDirect

Ore Geology Reviews

journal homepage: www.elsevier.com/locate/oregeorev

LA-ICP-MS analyses of trace elements in base metal sulfides from carbonate-hosted Zn-Pb deposits, South China: A case study of the Maoping deposit

Chen Wei [a,b], Lin Ye [a,*], Yusi Hu [a,b], Zhilong Huang [a], Leonid Danyushevsky [c,d], Haoyu Wang [a,b]

[a] State Key Laboratory of Ore Deposit Geochemistry, Institute of Geochemistry, Chinese Academy of Sciences, Guiyang 550081, China
[b] University of Chinese Academy of Sciences, Beijing 100049, China
[c] Centre for Ore Deposit and Earth Sciences (CODES), University of Tasmania, Private Bag 79, TAS 7001, Australia
[d] Transforming the Mining Value Chain (TMVC), Australian Research Council (ARC) Industrial Transformation Research Hub, University of Tasmania, Hobart, TAS 7001, Australia

ARTICLE INFO

Keywords:
Sichuan-Yunnan-Guizhou metallogenic province
Sulfides geochemistry
Physicochemical condition
Element partitioning
Ore genesis

ABSTRACT

The Sichuan-Yunnan-Guizhou metallogenic province (SYGMP) contains over 400 different size Zn-Pb deposits hosted in late Ediacaran to early Permian carbonate sequences and accounts for approximately 27% of the total Zn-Pb production in China. The Maoping deposit is a typical example that is not only mainly hosted in two different strata i.e., Devonian Zaige Formation (Fm.) and Carboniferous Baizuo Fm. but also shows a close spatial relationship with the Emeishan flood basalt. However, its ore genesis is poorly constrained. In this study, LA-ICP-MS trace element maps and spot analyses were generated on the sphalerite and galena selected from Maoping, aiming to establish tarce element partitioning behavior in co-crystallized sphalerite–galena, constrain the possible controls on the variation of trace element, and provide new insights into the ore genesis. The results show that Mn, Cd, Fe, Ge, Cu, In and Sn concentrations in sphalerite are higher than coexisting galena, yet galena is the preferential host for As, Ag, Sb, Tl, and Bi. The sphalerite from Carboniferous Baizuo Fm. is more concentrated in Cu, Ge, As, Ag and Sb than that of Devonian Zaige Fm., but has comparable trace element compositions to many other SYGMP Zn-Pb deposits hosted within the same sediment strata such as Huize and Tianqiao. This difference may be thought to have been controlled by host rock chemical composition with limited effect by physicochemical conditions and/or source(s) of metal elements. Sphalerite from the Maoping deposit is characterized by enrichments in Cd, Ge but depletions in Mn, Fe, In and Co, which are markedly distinct from that of the magma-related hydrothermal system (e.g., high-temperature (high-*T*) magmatic-hydrothermal, VMS and skarn deposits) but consistent with that of MVT deposits. Based on these results, together with the geological and geochemical features of the deposit, we considered that the Maoping Zn-Pb deposit belong to a MVT deposit.

1. Introduction

Carbonate-hosted epigenetic Zn-Pb deposits are widely distributed in the Yangtze carbonate platform (Zaw et al., 2007; Hu et al., 2017). For instance, approximately 400 Zn-Pb deposits have been found in the Sichuan-Yunnan-Guizhou (SYG) triangular area, accounting for approximately 27% of total zinc and lead production in China (Liu and Lin, 1999). These deposits are hosted within carbonate rocks of Late Ediacaran to Early Permian in age, including the world-class Huize (>7.0 Mt Zn and Pb; Huang et al., 2004), Daliangzi (~4.5 Mt Zn and Pb; Zheng and Wang, 1991), Maozu (~2.0 Mt Zn and Pb; Zhou et al., 2013a) and Tianbaoshan deposits (~2.6 Mt Zn and Pb; Zhang et al., 2015). Extensive researches have focused on those Zn-Pb deposits which are hosted in the Late Ediacaran-Cambrian and Carboniferous carbonate sequences, to document their geological characteristics, mineralization age and tectonic setting (e.g., Zheng and Wang, 1991; Huang et al., 2004; Li et al., 2007; Zhou et al., 2013a; Zhang et al., 2015; Hu et al., 2017; Bao et al., 2017), yet their Devonian carbonate-hosted counterparts have not been extensively studied during the past decades, leading to persisting uncertainties with respect to their ore genesis.

The Maoping deposit at the central part of the SYGMP (Fig. 1) is the largest deposit where the main orebodies are hosted within the

* Corresponding author.
E-mail address: yelin@vip.gyig.ac.cn (L. Ye).

https://doi.org/10.1016/j.oregeorev.2020.103945
Received 1 April 2020; Received in revised form 9 December 2020; Accepted 16 December 2020
Available online 19 January 2021

Devonian Zaige Fm. and Carboniferous Baizuo Fm. This deposit has an estimated ore resource >25 Mt, with an average grade of 15–35 wt% Zn + Pb (Wei et al., 2015). Several notable studies have been carried out on the Maoping deposit, most of which have been published in local Chinese literature. Despite its economic significance, its ore genesis is still controversial. The Zn-Pb orebodies show a close spatial relationship with the Emeishan flood basalt, leading to a great number of authors considering it as a distal magmatic-hydrothermal deposit associated with the Emeishan mantle plume (e.g., Liu, 1995; Wang, 2001; Xu et al., 2014). On the other hand, the deposit shows similar geological characteristics with typical MVT deposits. Therefore, several authors have regarded it as an MVT deposit (e.g., Zhang et al., 2015; Wei et al., 2015). There has not been, until now, a complete understanding of the Zn-Pb mineralization in the Maoping deposit.

Many studies have correlated compositional variations in sphalerite minerals with its geological environment (e.g., Kelley et al., 2004; Gagnevin et al., 2014; Cugerone et al., 2018; Wei et al., 2019) and origin (e.g., Zhang, 1987; Cook et al., 2009; Ye et al., 2011; Frenzel et al., 2016). The application of LA-ICP-MS allows in-situ analysis of various trace elements in sulfides with relatively low detection limits (e.g., Watling et al., 1995; Cook et al., 2009; George et al., 2015). These investigations demonstrated that trace element in sulfides can provide significant information on the origin of ore deposit (Cook et al., 2009; Ye et al., 2011, 2016; Frenzel et al., 2016; Wei et al., 2018) and the characteristics of the mineralizing fluid (e.g., Kelley et al., 2004; Wei et al., 2019). They can also be applied to exploration for Zn-Pb deposits (e.g., Gagnevin et al., 2014; Wei et al., 2019). In this paper, LA-ICP-MS spot and mapping analyses were used to determine sphalerite and galena trace element compositions in the Maoping Zn-Pb deposit in Yunnan, China. The new dataset allows us to 1) understand elemental partitioning behavior of sphalerite–galena assemblage in the low-temperature(low-*T*) hydrothermal system; 2) constrain possible controls on the observed compositional variation in sphalerite and 3) when combined with trace elements in sulfides, geology and previous studies, we provide new insight into the ore genesis of the Maoping deposit.

2. Geological setting

The Sichuan-Yunnan-Guizhou (SYG) triangle district, located within the southwestern margin of the Yangtze Block (Fig. 1A), covers over 170,000 km^2 and consists of the southwestern Sichuan Province, northeastern Yunnan Province and northwestern Guizhou Province (Liu and Lin, 1999). The triangle district is confined by the NW-trending Weining-Shuicheng, the SN-trending Anninghe and the NE-trending Mile-Shizhong regional fault belts (Fig. 1B). These three belts extend deep into basement rocks and have been activated and reactivated by a series of tectonic events, such as the Hercynian, Indosinian, Yanshanian and Himalayan orogenic events. A set of secondary NE-trending and NW-trending faults and thrust faults are well developed in this district.

In the SYG region, exposure stratigraphy are dominated by the Mesoproterozoic to Early Neoproterozoic basement overlain by the middle Neoproterozoic weakly metamorphosed strata, Late Neoproterozoic unmetamorphosed Ediacaran, early Mesozoic submarine sedimentary sequences, and Jurassic to Cenozoic terrigenous sediments. In addition, the Emeishan Mantle plume formed the remarkable Emeishan Large Igneous Province during late Permian (~260 Ma, He

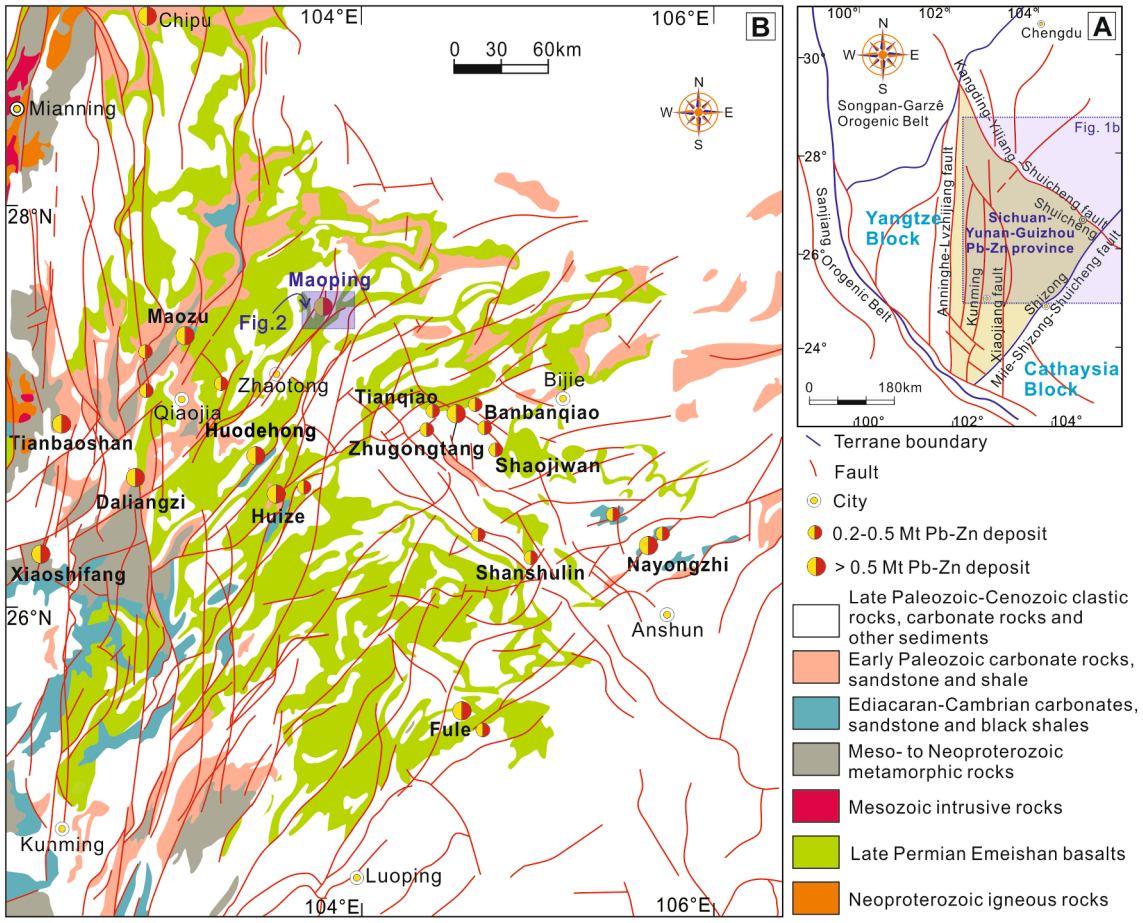

Fig. 1. (A). The tectonic setting of the western Yangtze Block, SW China; Simplified geological map of the South China Craton and adjacent regions showing the framework and the distribution of carbonate-hosted Zn-Pb deposits in the upper Yangtze Block (modified after Ye et al., 2011). (B). Geological map of the Sichuan-Yunnan-Guizhou metallogenic province (SYGMP) showing the locations of zinc-lead deposits (modified after Lin and Liu, 1999 and Xiang et al., 2020).

et al., 2007) in this district, covering an area of over 250,000 km^2. Detailed descriptions of exposed strata in the SYG triangle district can be found in Huang et al. (2004) and Zhang et al. (2015).

Carbonate-hosted Zn-Pb deposits are widely distributed in this district (Fig. 1B) and are featured by irregular orebodies, simple mineral assemblage, weak wall rock alteration, and high ore grade of Pb and Zn metals associated with the enrichment of Ag, Ge, Cd, Ga and In. Recent Rb-Sr dating sphalerite and Sm-Nd dating hydrothermal calcite/fluorite indicate that the majority of carbonate-hosted Zn-Pb deposits occurred between 226 Ma and 191 Ma (e.g., Li et al., 2007; Lin et al., 2010; Zhou et al., 2013b; Zhang et al., 2015 and references therein). This result shows the Zn-Pb mineralization in the SYG district is likely related to the Indosinian orogenic event.

3. The geology of Maoping deposit

3.1. Stratigraphy and lithology

The exposed strata around the Maoping deposit are composed of Silurian, Devonian, Carboniferous and Permian (Fig. 2). The Silurian strata consist of shale, sandstone and argillaceous sandstone. The Lower Devonian strata comprises sandstone, mudstone and dolostone, and overlies the Late Devonian Zaige Fm. dolostone with abundant sedimentary pyrite. The strata of Lower Carboniferous Datang and Baizuo Fms. are composed of limestone with thin layer of shale and dolostone interlayer with ~3 m thick clay shale, respectively. The Middle Carboniferous Weining Fm. conformity overlies the Lower Carboniferous Baizuo Fm. and mainly consists of limestone and dolostone. The Lower Permian Liangshan Fm. comprises shale and sandstone and overlies the Lower Permian Qixia and Maokou Fms. limestone. Additionally, the Emeishan flood basalts are widespread outside of the mining area.

3.2. Structure

The Maoping district is characterized by a set of NE- to NW-trending faults (Fig. 2). The NE-trending thrust faults mainly include the Maoping, Luozehe and Fangmaba faults, which are separated by a set of NW-trending faults. Specifically, the Maoping fault has a strike of NE10°–80° and a dip of SE65°–85° with 30 km long. The Luozehe fault strikes NE30°–40°and dips steeply at SE65°–70° with a length of >40 km. The Fangmaba fault strikes NE25° and dips SE67°–85° with a length of >20 km. The Maomaoshan inverted anticline is mainly the ore-control structure (Fig. 3A). Its fold axis has a variable strike: NW350° in its western wing and NE20°–45°in its northern wing. Its western wing are overturned with a dip of 65°–86°, while the eastern wing is relatively gentle dip (17°–35°).

3.3. Zn-Pb mineralization

Sulfide orebodies at Maoping occur as steeply plunging pipe-shaped bodies and are mainly hosted within the overturned NW wing of the Maomaoshan anticline. Post-ore NW-trending faults induced that the sulfide orebodies occur weakly deformation rather than metamorphism (Wang, 2018). Individual pipes have been grouped into the three larger orebodies, including Orebody I, Orebody II and Orebody III (Fig. 3B). Orebody I, the largest orebody, is hosted within the Devonian Zaige Fm., and 280–340 m in length, 5–34 m in width and 800 m in thickness with average ore grades of 13.0 wt% Zn, 7.5 wt% Pb and 135 g/t Ag. The second-largest Orebody II is hosted within the Lower Carboniferous Baizuo Fm., and is 20–182 m long, 22 m wide and 540 m thick with average ore grades of 16.0 wt% Zn and 6.0 wt% Pb. Orebody III is hosted within the interformational faulted zone of the Lower Carboniferous Weining Fm. The orebody is 43–202 m in length, 5 m in width and 170 m in thickness with average ore grades of 7.6 wt% Zn and 9.0 wt% Pb. Wall rock alterations in Maoping are principally dolomitization and calcitization, which are closely associated with Zn-Pb mineralization.

3.4. Mineralogy, texture and mineral paragenesis

Both sulfide and supergene ore are developed in the Maoping deposit. Primary sulfide minerals are relatively simple and are pyrite, sphalerite and galena (Figs. 4 and 5). Hydrothermal dolomite, calcite, and minor quartz occur as gangue minerals. The supergene ore is composed of smithsonite, hydrozincite, cerussite, hemimorphite and goethite (Zhou and Li, 2005).

Sulfide ores mainly occur as massive (Fig. 4A-B, D-E), veins (Fig. 4C, H), branded (Fig. 4F-G) and disseminated (Fig. 4I) in the Maoping

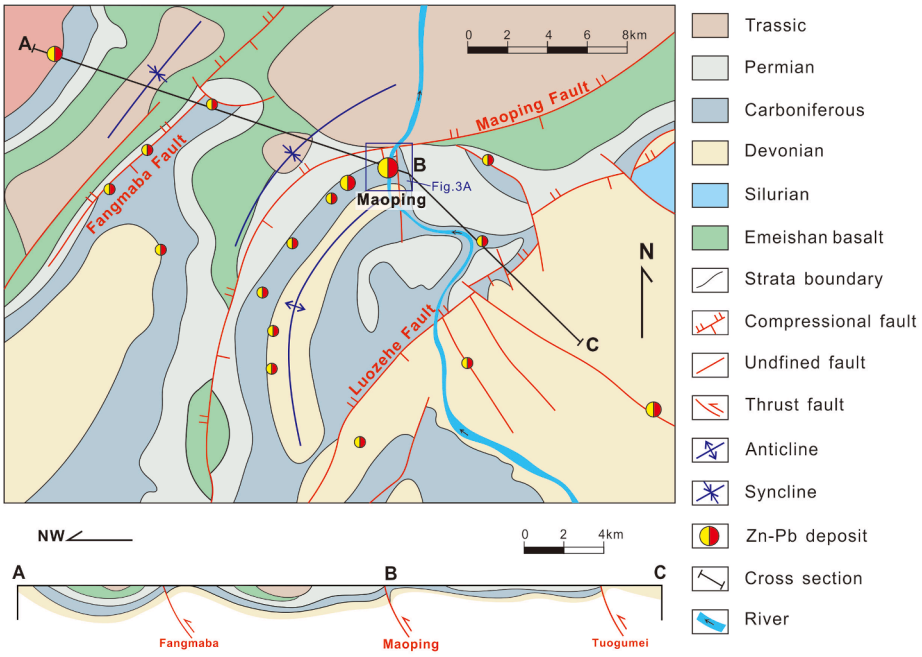

Fig. 2. Geological map of the Maoping district showing the stratigraphy, structure and the distribution of Zn-Pb deposits (modified after Liu and Lin, 1999).

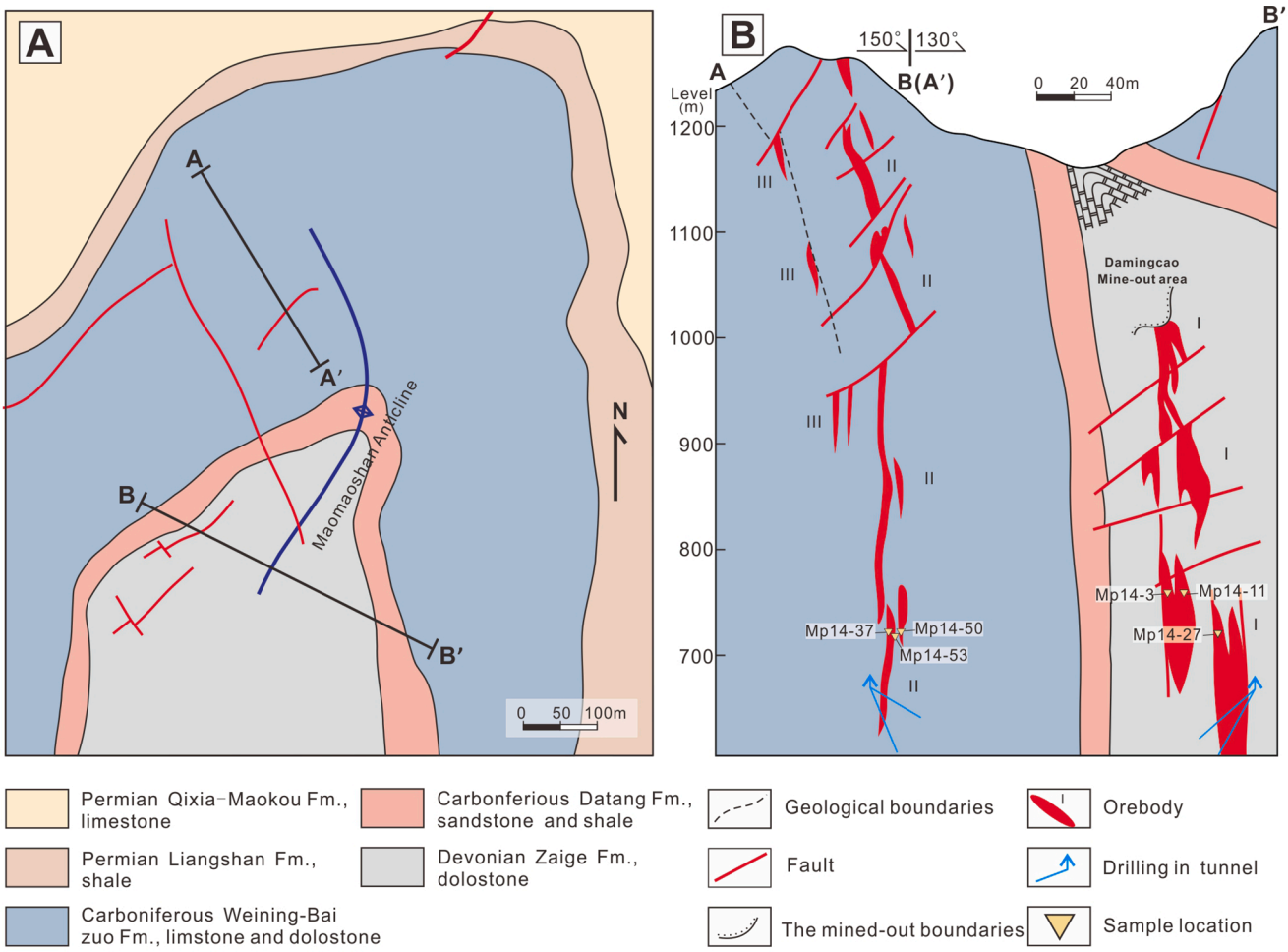

Fig. 3. (A). Geological map of the Maoping deposit. (B). Cross-section through the Maoping Zn-Pb deposit (modified after Liu and Lin, 1999).

deposit. The principal ore textures are euhedral-subhedral granular, veinlet-vein filling, and metasomatic texture. The pyrite usually occurs as euhedral to anhedral fine-medium grained minerals (Fig. 5A-C, H), and is enclosed and/or corroded by late sphalerite (Fig. 5A-B). It is common that pyrite is replaced by sphalerite (Fig. 5B-C) or galena (Fig. 5I). In some cases, the fine-grained pyrite assemblage filling the fracture of sphalerite is also observed (Fig. 5H).

The sphalerite is the principal mineral of this deposit, which is characteristically coarse-grained, euhedral-subhedral granular (0.5–10 mm) and replaced by galena (Fig. 5E, G, H). In some cases, sphalerite corrodes galena grain and forms irregular contact boundaries (Fig. 5D). It also occurs in metasomatic relict (Fig. 5E, G) and cataclastic texture (Fig. 5A, E). The galena is subhedral-anhedral granular and vein, which dissolute and replaces the early sphalerite or quartz (Fig. 5E, G, H). In some case, galena crosscut and replace the early pyrite (Fig. 5C, I). In addition, the calcite and hydrothermal dolomite fill in the fracture/vug of sulfide, i.e., pyrite (Fig. 4B), sphalerite (Fig. 4B, E) and galena (Fig. 4E). Euhedral quartz is enclosed or corroded by sulfides and randomly distributed within the sulfide matrix (Fig. 5A, D-E).

Based on detail field geology, hand-specimens and thin-section microscopic observations, a paragenetic sequence for the Maoping deposit was developed (Fig. 6). The mineralization process has been divided into three stages: early ore-stage, main ore-stage and late ore-stage. Early ore-stage, referred to as “the pyrite-quartz stage”, mainly contains pyrite and quartz. Fine euhedral pyrite is disseminated the wall rock, accompanied by minor quartz. Main ore-stage is economically the most important. A complex sulfide assemblage (sphalerite and galena) co-precipitated with hydrothermal dolomite. Paragenetically late ore-stage is composed of galena, minor pyrite, and co-precipitated with hydrothermal dolomite and calcite.

4. Approach and experimental methods

4.1. Analytical sample from the Maoping deposit

Ore samples from the Maoping Zn-Pb deposit were collected from two orebodies, including 3 samples from Orebody I and 3 samples from Orebody II. The details are listed in Table 1 and the sample locations are shown in Fig. 3B. Each sample was prepared as a one-inch polished block and characterized by optical microscopy and back-scattered electron (BSE) imaging prior to LA-ICP-MS analysis. Only areas of sphalerite and galena grains free of noticeable inclusions were selected for LA-ICP-MS analysis.

4.2. LA-ICP-MS analysis

LA-ICP-MS spot and mapping analyses were conducted at the CODES laser ablation analytical facility, University of Tasmania (Hobart, Australia), using a high-performance RESOlution 193 nm ArF excimer Laser Ablation System coupled to an Agilent 7700x Quadrupole ICP-MS. The ablated aerosol was transported using a constant He flow and mixed with Ar in a cyclone coaxial mixer before entering the ICP-MS.

Pre-defined areas of the polished blocks were ablated at a 30 μm spot size with a repetition rate of 10 Hz and energy set to produce a fluence at the sample of 5–6 J/cm^2. Analysis time for each sample comprises 30 s laser-off background measurement and 60 s laser-on sample analysis.

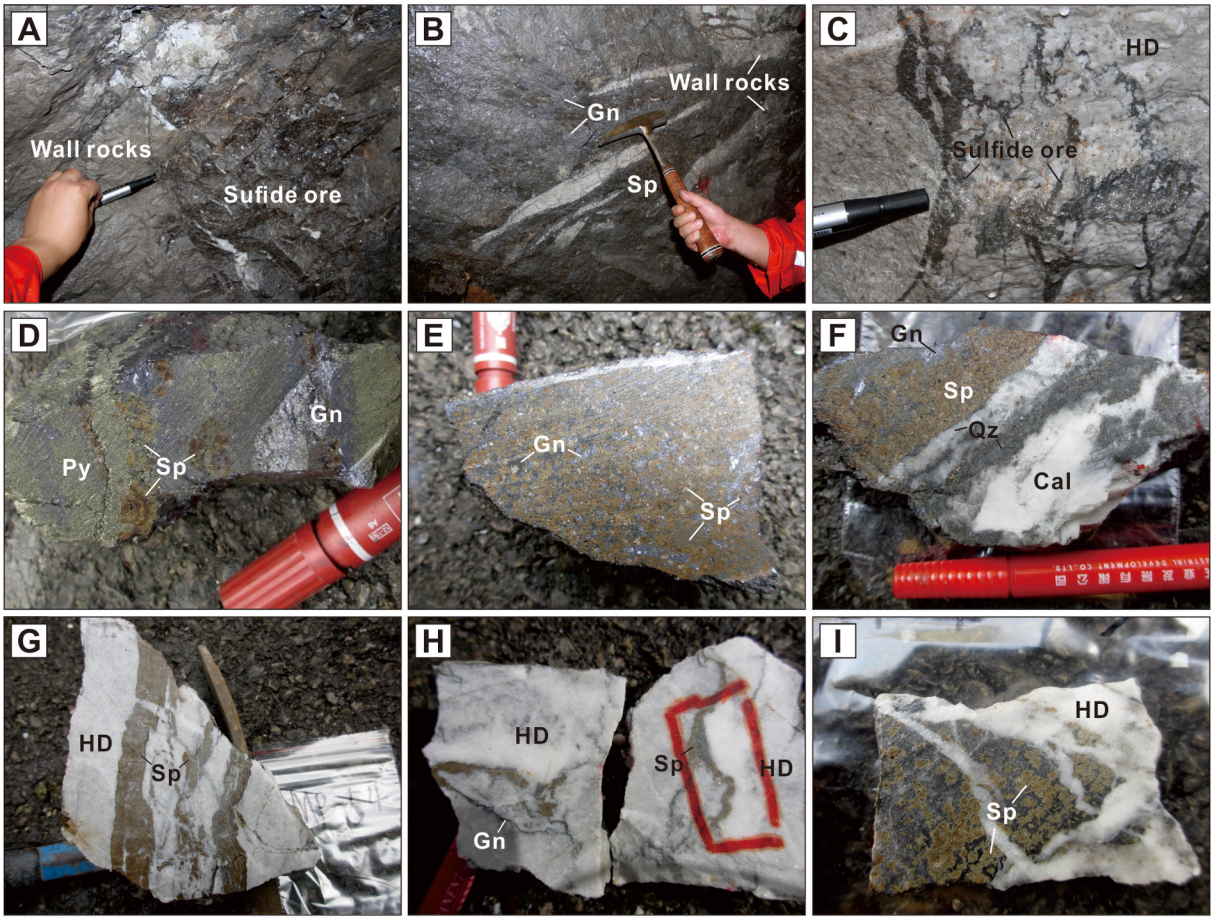

Fig. 4. (A). The clear boundary between the host rock and massive sulfide ore. (B). A small volume of host rocks was enclosed by the massive sphalerite-galena assemblage. (C). Sulfide veinlets occur within the hydrothermal dolomite. (D). Massive sulfide ore containing pyrite, sphalerite, and galena. (E). Sphalerite overgrows with galena in the specimen. (F). Massive sphalerite-galena-quartz assemblage was commented by late calcite. (G). Banded sphalerite parallel with hydrothermal dolomite. (H). Sphalerite veins occur within the hydrothermal dolomite. (I). Speckled sphalerite randomly distributed within the host rocks and then crosscut by late hydrothermal dolomite. Abbreviation: Py = pyrite, Gn = galena, Sp = sphalerite, Qz = quartz, Cal = calcite, HD = hydrothermal dolomite.

Data were collected using time-resolved mode. The following isotopes were monitored: ^{34}S, ^{55}Mn, ^{57}Fe, ^{59}Co, ^{60}Ni, ^{65}Cu, ^{66}Zn, ^{72}Ge, ^{74}Ge, ^{75}As, ^{77}Se, ^{107}Ag, ^{109}Ag ^{111}Cd, ^{115}In, ^{118}Sn, ^{121}Sb, ^{205}Tl, ^{206}Pb, ^{208}Pb and ^{209}Bi. The dwell time for Ni, Se, Tl and Bi were set to 0.05 s while all other elements were set to 00.2 s. Calculation of mass fractions and correction for instrument drift were carried out using the in-house sulfide standards STDGL2b2 (Danyushevsky et al., 2011) and GSD-1G (USGS, USA). Data reduction calculations and error propagations were performed using LADR software designed at CODES, following the standard methods of Longerich et al. (1996). Galena was assumed to be stoichiometric and processed using an internal standard of 86.6% Pb. Sphalerite was processed using an assumed internal standard of 63.6% Zn analyzed by EMPA. The complete trace elements dataset, the minimum detection limits (mdl) and analytical accuracy for each element in each sample are given in Electronic Appendix A.

LA-ICP-MS images of sphalerite and galena were carried out by ablating sets of parallel line rasters in a grid across the sample. A consistent laser spot size (12 μm) and 10 μm/s scan speed were chosen to ensure the desired sensitivity for the elements of interest, as well as adequate spatial resolution. The spacing between the lines was adjusted to match the laser spot size. A laser repetition of 10 Hz was selected at a constant energy output of 100 mJ. Fifteen elements were analyzed with the dwell time set to 0.02 s for all elements. A 30 s of background was acquired by the ICP-MS before each line was ablated, followed by a delay of 20 s for cell wash-out, gas stabilization, and computer processing time. Identical rasters were done on the reference materials of STDGL2b2 and GSD-1G at the start and end of a mapping run to calculate element concentrations in sphalerite and galena, and to correct for instrumental drift, if necessary. Element maps were compiled and processed using the program Iolite developed by the Melbourne Isotope Group (Paton et al. 2011), an open-source software package for processing ICP-MS data, and an add-in for the data analysis program Igor developed by WaveMetrics. All LA-ICP-MS maps were produced for each element using a logarithmic color scale.

5. Results

Trace elements in main ore-stage mineral assemblage (sphalerite and galena) selected from two orebodies analyzed by LA-ICP-MS are summarized in Table 2. The dataset consists of 25 spots of sphalerite and 14 spots of galena analyses in Orebody I, 24 spots of sphalerite and 8 spots of galena analyses in Orebody II (data listed in Electronic Appendix A). LA-ICP-MS ablation profiles were generally smooth, indicating a homogeneous distribution of elements in the spot analyzed (Fig. 7). The results show that the samples of two orebodies are provided with different trace element compositions (Fig. 8).

5.1. Trace and minor element in sphalerite

Sphalerite displays significant Fe content (1.37–5.19 wt%, averaging 2.74 wt%; Table 2 and Fig. 8A) which is relatively enriched in Orebody I, with a geometric mean of 3.15 wt%.

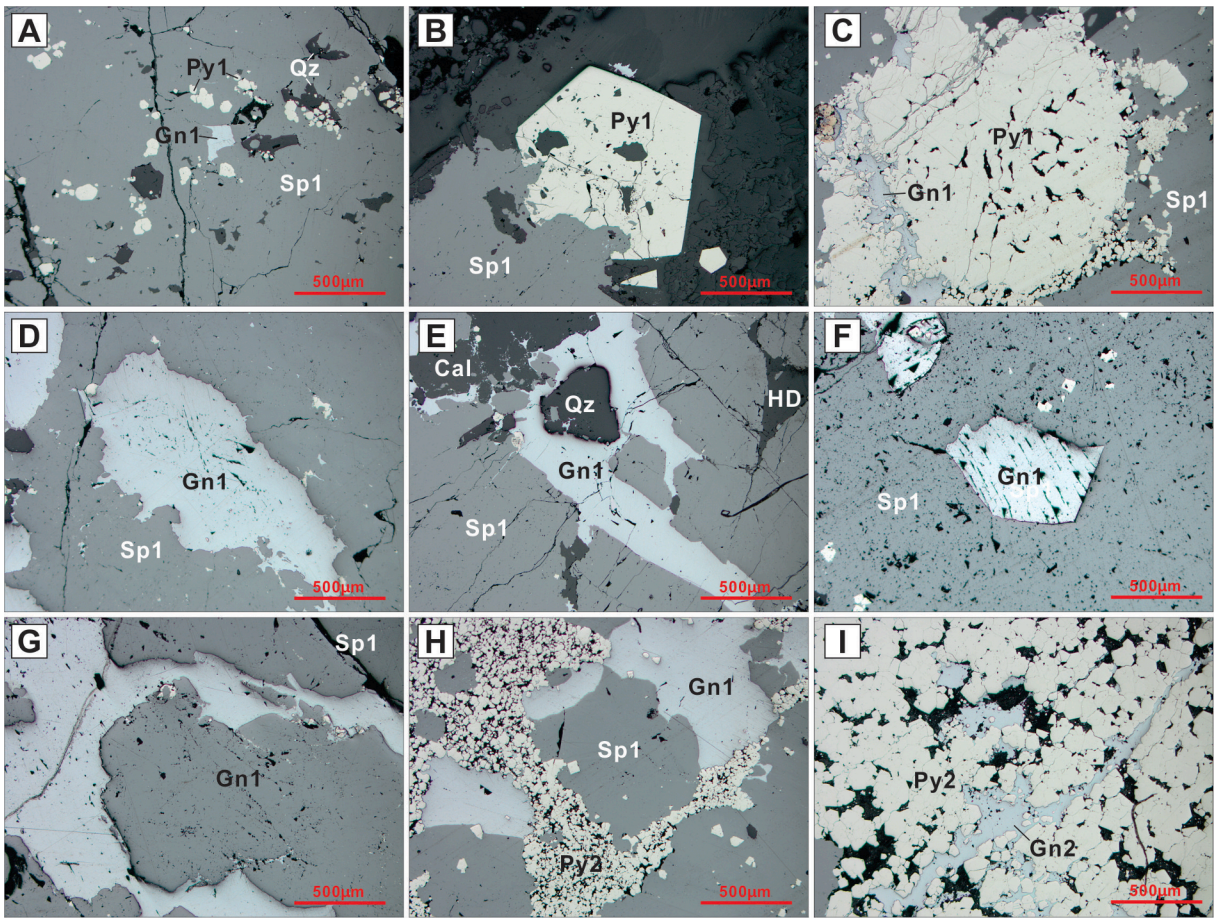

Fig. 5. (A). Fine-grained Py1 and Gn1 inclusions randomly distributed in the Sp matrix. (B). Euhedral Py1 was replaced by late Sp1. (C). Py1 crosscut Gn1 and then enclosed by late Sp1. (D). Sp1 dissolves the early Gn1, forming irregular boundaries between Sp1 and Gn1. (E). Gn1 vein replaces early Qz and then crosscuts the Sp1. (G). Sp1 is co-crystalized with Gn 1. F. Gn1 dissolves the Sp1 and forms the irregular edge. (H). Sp1 overgrows with Gn1 and then crosscut by fine-grained Py2 aggregate. (I). Gn2 veins crosscut the fine-grained Py2 aggregate. Abbreviation: Py = pyrite, Gn = galena, Sp = sphalerite, Qz = quartz, HD = hydrothermal dolomite.

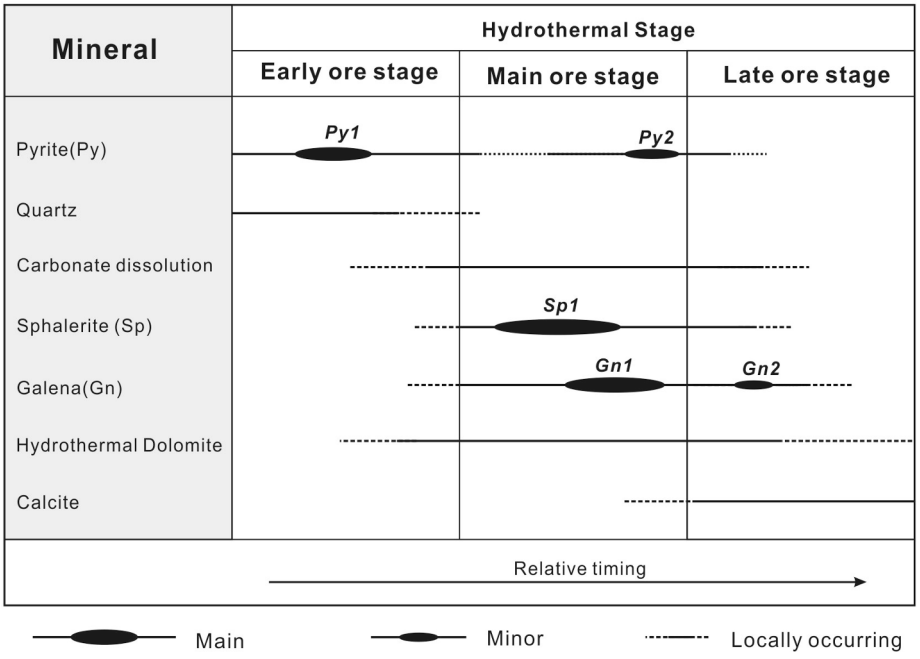

Fig. 6. Mineral paragenesis in the Maoping deposit.

Table 1
Brief description on the six samples selected from the Maoping deposit.

Sample No.	Location	Description	Mineral assemblages
Mp14-3	Orebody I, level 760 m	Py-Gn thin vein crosscut the massive Sp	Sp, and minor Gn and Py
Mp14-11	Orebody I, level 760 m	Massive Sp ore replaced by Py and Gn veinlets	Sp, Gn, Py and minor HD
Mp14-27	Orebody I, level 720 m	Coarse-grained Py enclosed and/or replaced by late Sp and Gn	Sp, Py and Gn
Mp14-37	Orebody II, level 720 m	Euhedral Py enclosed by disseminated Sp and Gn	Sp, Py and minor Qz
Mp14-50	Orebody II, level 720 m	Sp-Py thin veins occur within hydrothermal dolomite	Sp, Py and HD
Mp14-53	Orebody II, level 720 m	Quartz crystals were filled by Sp-Gn veins and forming chickenwire texture	Sp, Gn, HD and minor Qz

Notes: Definitions of mineral abbreviations: Sp = sphalerite; Gn = galena; Py = pyrite; HD = hydrothermal dolomite; Qz = quartz

Considering trace elements, Cd content shows quite similar distribution in two orebodies (1245–2214 ppm in Orebody I and 1225–2005 ppm in Orebody II, respectively). Trace elements like Cu, Ag, Ge and As vary over two orders of magnitude (10.8–1956 ppm, 7.27–84.9 ppm, 0.37–652 ppm and < mdl to 79.6 ppm, respectively) and are largely concentrated in Orebody II, with a geometric mean of 92.1 ppm, 42.6 ppm, 15.9 ppm and 15.8 ppm, respectively. Mn concentration displays relatively narrow range (10.4–62.0 ppm), and more concentrated in Orebody I, with a geometric mean of 38.9 ppm. The contents of In, Sb, Sn and Pb respectively extend from < mdl to 563 ppm, <mdl to 334 ppm, <mdl to 116 ppm and < mdl to 52.7 ppm. In and Sn are relatively enriched in Orebody I, with a geometric mean of 1.16 ppm and 1.21 ppm, respectively; whereas Sb and Pb are relatively enriched in Orebody II, with a geometric mean of 13.3 ppm and 13.1 ppm, respectively. Co and Tl display approximately the same range of concentration. Co presents in a remarkable higher concentration in Orebody I (geometric mean of 0.32 ppm), while Tl are more concentrated in Orebody II (geometric mean of 0.11 ppm). Further, among the elements analyzed in this study, Ni, Se, Tl, and Bi have been detected in a few spots with contents mostly below the mdl.

5.2. Trace element in galena

Ag and Sb have mostly considerable concentration in galena from the Maoping deposit with respect to any other elements analyzed in this study (Table 2 and Fig. 8B), with the content ranging from 229 ppm to 1321 ppm and 224 ppm to 29651 ppm, respectively. Sb is relatively enriched in Orebody I, with a geometric mean of 4467 ppm; whereas Ag shows quite similar distribution in two orebodies (geometric mean of 789 ppm in Orebody I and 847 ppm in Orebody II, respectively). As and Tl concentrations vary over two orders of magnitude from < mdl to 1030 ppm and 4.16 ppm to 160 ppm, respectively and are relatively enriched in Orebody I (Table 2 and Fig. 8B). The contents of Cu, Cd, Sn, Ge and Bi respectively extend from < mdl to 9.49 ppm, 1.23 ppm to 11.2 ppm, <mdl to 0.70 ppm, <mdl to 0.40 ppm and 0.02 ppm to 6.26 ppm. Ge and Cd display a roughly similar variation between Orebody I and Orebody II. Whereas Cu, Sn and Bi more concentrated in Orebody I, with a geometric mean of 1.8 ppm, 0.15 ppm and 0.17 ppm, respectively. In addition, the contents of Fe, Co, Ni, In and Se in galena are mostly below the mdl.

5.3. LA-ICP-MS element mapping

Trace element maps in a co-crystallized galena–sphalerite from the Maoping deposit are shown in Fig. 9. Trace elements like Fe, Cu, Cd, Ge and Sn are all mainly concentrated in sphalerite, whereas Ag, Sb, Tl and probably Bi are all primarily concentrated in galena. Moderate concentration of Mn and Sn are present in sphalerite, and some Cd is noted in galena. In addition, LA-ICP-MS element mapping also shows low levels of indium in sphalerite. Ge, Cu, Ag, Sb and Sn display erratic distribution within sphalerite, which may be indicative of zonation. Fracture present in sphalerite concentrates moderate Pb and As.

6. Discussion

6.1. Physicochemical condition of ore formation

Many studies have demonstrated that trace element compositions of sphalerite show inmate relationship with the temperature of ore formation (Oftedahl, 1940; Möller, 1987; Kelley et al., 2004; Frenzel et al.

Table 2
LA-ICP-MS results in the sphalerite and galena samples from different orebodies.

		Mn	Fe	Co	Ni	Cu	Zn	Ge	As	Se	Ag	Cd	In	Sn	Sb	Tl	Pb	Bi
Sphalerite from Orebody I (n = 25 in 3 samples)	Count	25	25	19	1	25	–	25	12	4	25	25	24	24	21	9	23	6
	Max	62.0	5.41	2.17	0.27	378	–	147	48.7	2.97	84.9	2214	563	13.2	45.1	0.26	76.9	0.25
	Min	19.3	1.81	0.01	–	10.8	–	1.21	1.45	2.03	7.27	1245	0.04	0.11	0.30	0.02	0.19	0.01
	Median	40.3	2.96	0.51	–	42.1	–	7.95	1.97	2.51	23.1	1563	0.29	0.89	2.17	0.05	8.96	0.02
	GM	38.9	3.15	0.32	–	57.8	–	10.2	3.44	2.47	26.2	1573	1.16	1.21	2.23	0.06	6.15	0.03
	S.D.	13.7	1.03	0.70	–	105	–	35.8	17.4	0.49	20.9	249	136	3.79	12.6	0.08	23.7	0.09
Galena from Orebody I (n = 14 in 2 samples)	Count	–	2	4	4	13	4	9	13	3	14	14	6	13	14	14	–	14
	Max	–	15.7	1.20	0.11	9.49	31.3	0.40	1029	35.0	1321	11.2	0.02	0.70	29,651	160	–	6.26
	Min	–	6.72	0.01	0.01	0.19	0.53	0.16	1.72	2.31	229	1.23	0.001	0.05	224	4.50	–	0.02
	Median	–	–	0.04	0.04	2.07	1.57	0.20	18.5	2.81	866	9.59	0.01	0.11	5257	6.72	–	0.16
	GM	–	10.3	0.05	0.04	1.83	2.52	0.21	26.4	6.11	789	7.69	0.004	0.15	4467	8.80	–	0.17
	S.D.	–	6.34	0.59	0.04	2.79	15.1	0.07	291	18.7	258	2.77	0.01	0.21	10,520	40.9	–	1.94
Sphalerite from Orebody II (n = 24 in 3 samples)	Count	24	24	22	1	24	–	23	14	3	24	24	20	22	22	14	24	2
	Max	33.2	3.65	0.22	0.11	1956	–	652	79.6	3.51	74.8	2005	1.06	52.7	334	0.48	116	0.01
	Min	10.4	1.34	0.03	–	18.5	–	0.37	3.70	2.12	20.0	1225	0.003	0.09	0.31	0.03	0.37	0.01
	Median	23.0	2.30	0.15	–	87.2	–	27.1	18.7	2.39	41.1	1486	0.14	0.52	15.7	0.10	15.8	–
	GM	21.8	2.13	0.11	–	92.1	–	15.9	15.8	2.61	42.6	1492	0.09	0.71	13.3	0.11	13.1	–
	S.D.	5.90	0.55	0.06	–	412	–	146	21.7	0.74	14.2	214	0.36	11.1	73.3	0.13	31.8	–
Galena from Orebody I and II (n = 8 in 1 sample)	Count	–	1	2	1	8	1	4	8	1	8	8	2	7	8	8	–	8
	Max	–	4.82	0.002	0.04	1.68	2.33	0.21	123	0.43	965	8.87	0.002	0.11	3892	5.93	–	0.30
	Min	–	–	0.001	–	0.24	–	0.16	1.43	–	678	6.44	0.002	0.03	917	4.16	–	0.03
	Median	–	–	–	–	1.33	–	0.19	25.6	–	881	8.03		0.05	2316	5.10	–	0.08
	GM	–	–	–	–	0.99	–	0.19	20.8	–	852	7.90		0.05	1964	5.05	–	0.08
	S.D.	–	–	–	–	0.53	–	0.03	38.3	–	100	0.72		0.03	1150	0.56	–	0.09

Notes: (1) Fe in wt.% and other elements in ppm in the data table; (2) the counts only contain the content > the minimum detection limits (mdl); (3) geometric mean (GM).

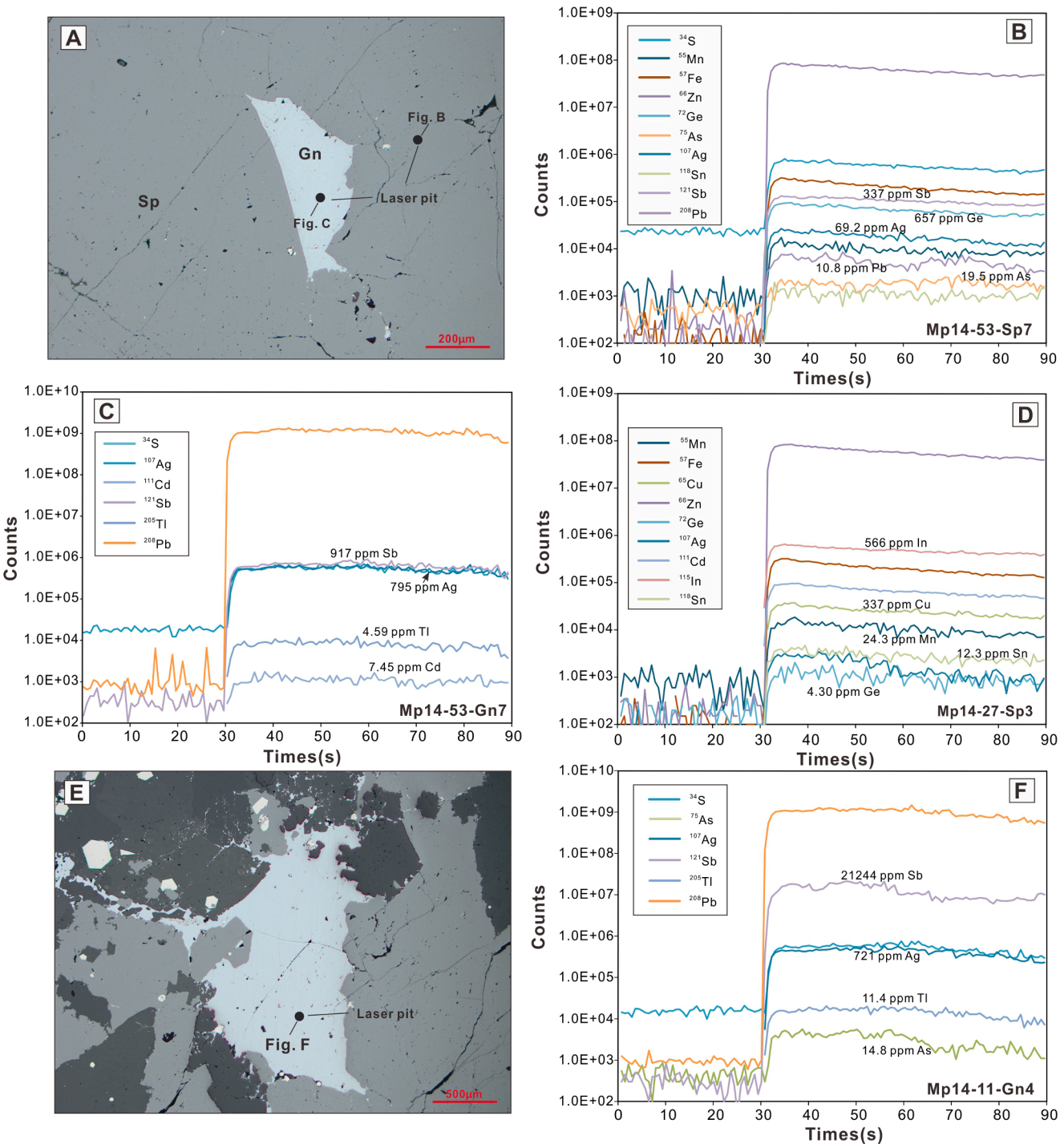

Fig. 7. Typical single-spot LA-ICP-MS spectra for selected elements in sphalerite and galena analyzed in this study. Numbers in brackets are concentrations (in ppm). (A). Reflected light photomicrograph shows the analyzed location of co-crystallized sphalerite and galena and correspond time-resolved depth profiles of sphalerite (B) and galena (C) in sample Mp14-53. (D). Smooth signals for all elements in high In sphalerite from Mp14-27. (E). The analyzed location of high Sb galena in sample Mp14-11, corresponding smooth spectra for Sb, Ag, As and Tl (F).

2016). For example, the concentrations of the In, Fe, Mn, Ga and Ge in sphalerite can be used to estimate the formation temperature of the Zn-bearing sulfide ores (Frenzel et al., 2016). Petrographic observation shows that sphalerite at Maoping is mostly red-brown and yellow in color and Fe content is 1.37–5.19 wt%, similar to the sphalerite formed at 100–200 °C (Kelley et al., 2004). Using the concentration of In, Fe, Mn and Ge in sphalerite from all sample and Ga contents (~20 ppm) of sphalerite according to Han et al (2012), the GGIMFis geothermometer (Frenzel et al., 2016) yield a mean homogenization temperature of 208 ± 16 °C for Orebody I and 196 ± 16 °C for Orebody II, respectively. This estimate is within an error of the microthermometric data of fluid inclusions of gangue minerals (170–247 °C; Han et al., 2007). Therefore, the sphalerite GGIMFis geothermometer confirms that the Maoping deposit formed under low-*T* conditions. Fe content in sphalerite can be used to suggest the temperature and fS_2 and/or fO_2 (Scott and Barnes, 1971; Scott, 1983; Hutchison and Scott, 1983; Kelley et al., 2004). The lower value of Fe content in sphalerite from both orebodies relative to the marmatite formed in high-*T* condition and accompanied with

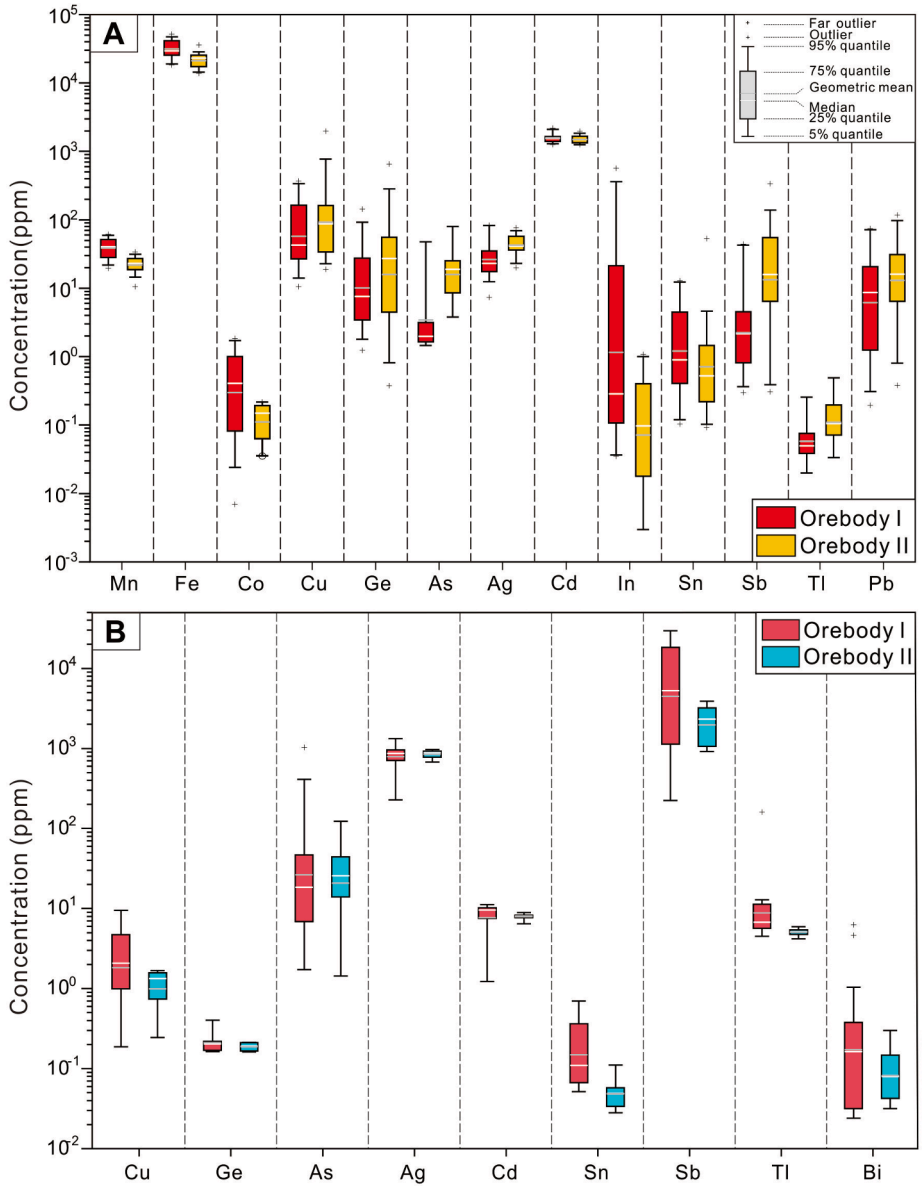

Fig. 8. Box and whisker plots of trace elements in sphalerite (A) and galena (B) from Orebody I and Orebody II of the Maoping deposit analyzed by LA-ICP-MS. The upper and lower threshold values (95%). The upper and lower margin of the box represent the upper 75% and 25% of the data. Geometric mean values are shown as solid gray lines and median values as solid white lines.

abundant pyrite (Fig. 4D, 5B-C), indicating the formation of sulfide ores at Maoping under medium–low temperature and low fO_2 conditions. This funding is also supported by the bulk gas composition of fluid inclusion. CH_4 and C_2H_6 have been detected in fluid inclusion of gangue minerals from both orebodies (Han et al., 2007), which further suggests a reduced environment during the sulfide precipitation.

6.2. *Element partitioning between sphalerite and galena*

Recently, several in-situ trace elements data have been published on the common sulfides (e.g., Kelley et al., 2004; Cook et al., 2009, 2011; Ye et al., 2011; Bauer et al., 2019). George et al. (2016) preliminary obtained the partitioning of trace element co-crystallized sphalerite, galena and/or chalcopyrite of the high-*T* (>300 °C) magma-driven hydrothermal deposits. However, the partitioning behavior of the sphalerite–galena assemblage in the low-*T* (<250 °C) hydrothermal deposits, such as carbonate-hosted Zn-Pb deposits, is poorly constrained. In this study, trace element spots and maps of co-crystallized sphalerite and galena from Maoping (~200 °C; this study) were analyzed by LA-ICP-MS aiming to exhibit the partitioning between sphalerite and co-crystallized galena.

The true partitioning coefficients among minerals may significantly be affected by non-equilibrium superimposed, remobilization and overgrowth process. Thus, it is necessary to examine petrographic and (micro-) textural when interpreting apparent element partitioning behavior (George et al., 2016). In the Maoping deposit, the relative lack of deformation in calcite veins and the generally good preservation of trace element zonation patterns in sphalerite (Fig. 9) indicate that the post-ore hydrothermal overprint is insignificant in the Maoping area (George et al., 2015; Wang, 2019). Thus, the sphalerite–galena assemblage from Maoping could be used to discuss the partition behavior of trace elements.

The concentrations of Mn, Fe, In, Sn and Bi in sulfides from Maoping are remarkably lower than that of reported high-*T* magma-driven hydrothermal deposits (George et al., 2016; Bauer et al., 2019). Nevertheless, the trace element partitioning pattern of sphalerite between

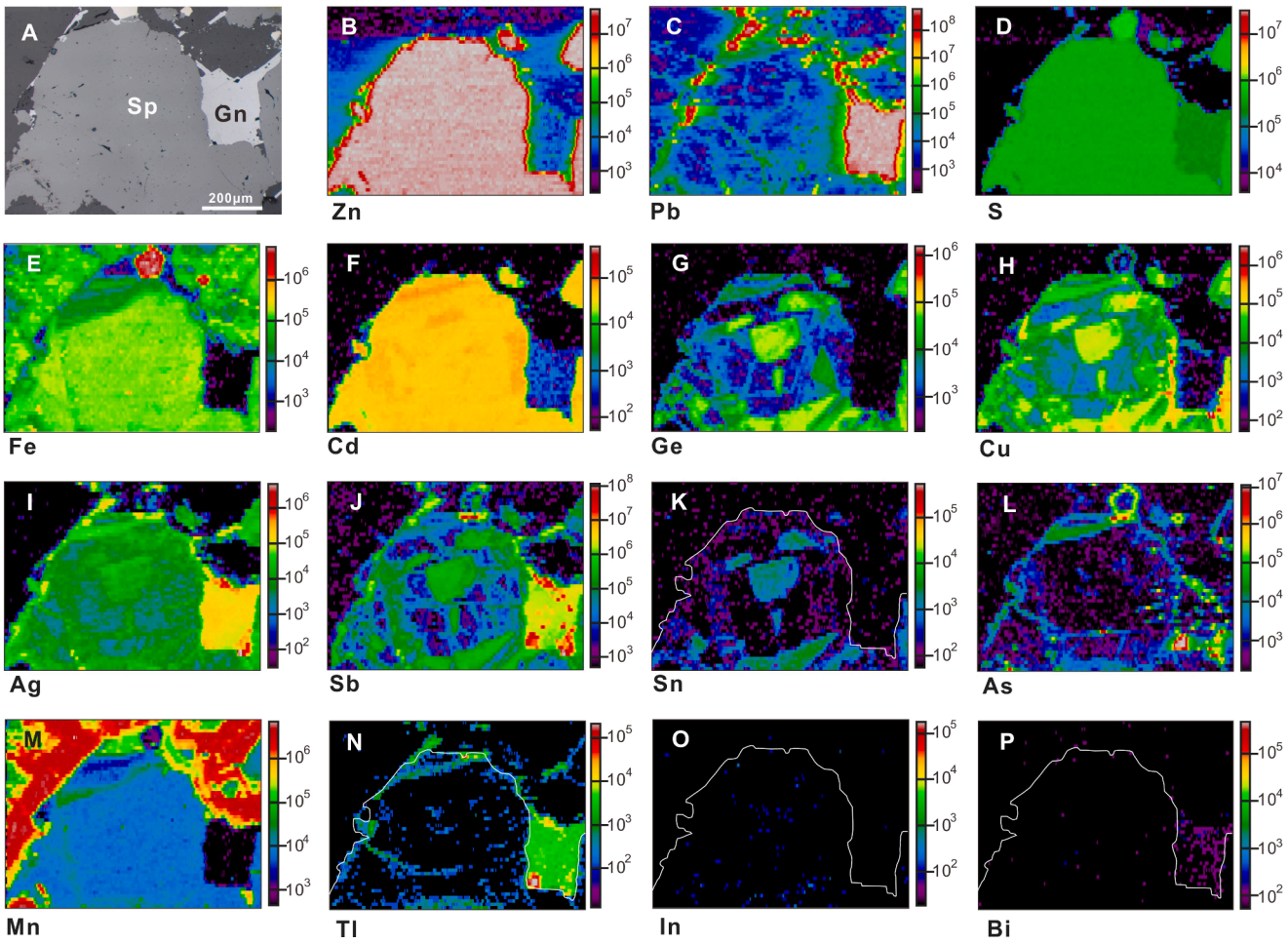

Fig. 9. Elemental maps generated with LA-ICP-MS show the distribution of selected trace elements in sphalerite from sample Mp14-53. (A). Reflected light photomicrograph of mapped sulfides that sphalerite coexisting with galena. (B–P). Different elements (Zn, Pb, S, Fe, Cd, Ge, Cu, Ag, Sb, Sn, As, Mn, Tl, In and Bi, respectively) of LA-ICP-MS maps. Scales in counts-per-second. Mineral abbreviations: Sp = sphalerite, Gn = galena.

galena coincident with the result of George et al. (2016). Mn, Fe, In and Sn preferred host within sphalerite and galena incorporates higher Bi (Table 3 and Fig. 9). The measured Cd and Cu concentrations in sphalerite from the Maoping deposit are generally one or more order of magnitude greater than galena, suggesting that sphalerite is the preferred host, consistent with previously published data (George et al., 2016; Ye et al., 2016; Hu et al., 2019). All LA-ICP-MS spot analyses show that high concentrations of Sb (>2.9 wt%) and Ag (>1300 ppm) were detected in galena (Table 2), together with smooth and flat time-resolved depth profiles (Fig. 7E-F), which may be explained by $AgSbS_2$-PbS solid solution. Our data also shows that Tl and As are always primarily concentrated in galena, with only a few spots of sphalerite samples contain the concentrations of Tl and As above the mdl (Table 3). This again indicates the galena is the primary host of Tl and As in sphalerite–galena assemblage of the low-*T* hydrothermal system, in agreement with George et al. (2016). Besides, compositional data and LA-ICP-MS element mapping display that sphalerite is the preferred hosted for Ge (up to 650 ppm) among all minerals (Fig. 9), in agreement with most earlier reports (e.g., Bernstein, 1985; Höll et al., 2007). In conclusion, the element partitioning between coexisting sphalerite and

Table 3
Trace element concentrations in co-crystallized sphalerite and galena determined by LA-ICP-MS spot analysis.

Sample Name	Sulfides		Mn	Fe	Co	Ni	Cu	Ge	As	Se	Ag	Cd	In	Sn	Sb	Tl	Bi
Mp14-11 (8)	Sphalerite	GM	50.9	45,734	0.11	–	54.9	38.1	5.41	–	38.6	1734	0.19	1.26	3.11	0.09	0.25
Orebody I		S.D.	6.48	4431	0.17	–	143	97.0	27.1	–	27.9	194	0.10	4.56	16.1	0.12	–
	Galena	GM	–	10.3	0.08	0.02	1.27	0.22	18.9	–	838	8.20	0.001	0.11	8101	7.76	0.05
		S.D.	–	6.34	0.85	0.02	1.82	30.7	27.3	–	121	2.08	0.001	0.22	11,660	3.17	0.06
Mp14-27 (6)	Sphalerite	GM	25.4	23,487	0.86	–	81.5	5.60	3.85	2.32	25.0	1355	57.5	3.80	1.91	0.07	0.02
Orebody I		S.D.	3.56	3935	0.57	–	108	8.54	19.2	0.47	13.6	74	200	3.79	2.19	0.05	0.002
	Galena	GM	–	–	0.04	0.07	2.79	0.21	39.0	6.11	728	7.06	0.01	0.23	2020	10.4	1.02
		S.D.	–	–	0.02	0.04	3.37	0.004	414	18.7	391	3.73	0.002	0.18	3927	63.0	2.610
Mp14-53 (8)	Sphalerite	GM	23.3	26,106	0.18	–	246	82.5	20.1	2.39	38.7	1675	0.01	0.66	25.7	0.09	0.01
Orebody II		S.D.	4.24	4820	0.03	–	646	219	29.2	–	14.8	228	0.01	2.03	111	0.07	–
	Galena	GM	–	4.82	0.001	0.04	0.99	0.19	20.8	0.43	847	7.90	0.002	0.05	1964	5.05	0.08
		S.D.	–	–	0.001	–	0.53	0.03	38.3	–	99.6	6.87	–	0.03	1150	0.56	0.09

Notes: (1) all elements in ppm in the data table; (2) the counts only contain the content > the minimum detection limits (mdl); (3) geometric mean (GM).

galena in the low-*T* Zn-Pb deposits share similar characteristics with the high-*T* magmatism-related deposits, suggesting that temperature and the ore deposit type show insignificantly influence on the element partitioning.

6.3. Control on compositional variation of sphalerite

As shown in Fig. 8A, sphalerite grains of sulfide ore selected from Orebody I have higher Mn, Fe, Co and In but lower Cu, Ge, As, Ag, Sb and Tl than those hosted in Orebody II. Slight variation in Fe and other elements difference between two orebodies is most likely influenced by 1) physicochemical conditions (e.g., temperature, fO_2 and pH) during mineral formation, 2) source reservoir of metal elements, and/or 3) host rock composition due to fluid-rock interaction (e.g., Bethke and Borton, 1971; Barton et al., 1977; Scott, 1983; Cook et al., 2009). As Section 6.1 mentioned, temperature and fO_2 of two orebodies at Maoping are very similar. Meanwhile, Pattrick et al. (1993) found that the change of pH between 5 and 6 shows a limited effect on the solubility of these elements (e.g., Cu, Fe, In, Cd, Zn) at 100–150 °C. Therefore, it is mean that the changes of physicochemical conditions (e.g., temperature, fO_2, and pH) shows very limited influence on distinct trace element contents between two orebodies.

The source reservoir of metal elements is considered to be major factors for the different trace element compositions of sphalerite between Orebody I and II. However, in-situ Pb isotope of sulfides from two orebodies is overlapped, suggesting metal elements were probably derived from the same source, i.e., metamorphic basement (e.g., Xiang et al., 2020), which is also supported by Zn and Cd isotope data (He, 2019). The source reservoir of metal elements thus played a very limited role in the abundances of these elements between two orebodies.

Host rock composition was likely important. Sulfides such as sphalerite formed during replacement or fluid-rock interaction may "inherit" some element characteristic of the host rocks (e.g., Doe and Delevaux, 1972; Wei et al., under review). The sulfide ore at Maoping is hosted dominantly in the Devonian Zaige Fm. (Orebody I) and Carboniferous Baizuo Fm. (Orebody II), respectively (Wang et al., 2009; Wei et al., 2015), which is an ideal case study for investigating the effect of host rock composition on sphalerite chemistry. Petrographic observations show the Maoping deposit occurs intense water–rock interaction which could dissolve and leach the portion of sediment constituents (e.g., metal, C and O elements) from host rocks (Fig. 4A-C), and involve in sulfide mineralization (Wei et al., 2015). Meanwhile, the whole-rock compositions of two orebodies show significant differences as described in the Section "Geology of the Maoping deposit". Slight higher Fe and Co in sphalerite from Orebody I relative to that of Orebody II is attributed to sedimentary pyrite which occurs the Devonian Zaige Fm. While the interlayer thin clay shale of the Carboniferous Baizuo Fm. contain abundant Cu, Ge, As, Ag and Sb (Guo, 2011), which could be the main factor for sphalerite from Orebody II enriched these elements than that from Orebody I, in agreement with the difference of Sn in galena

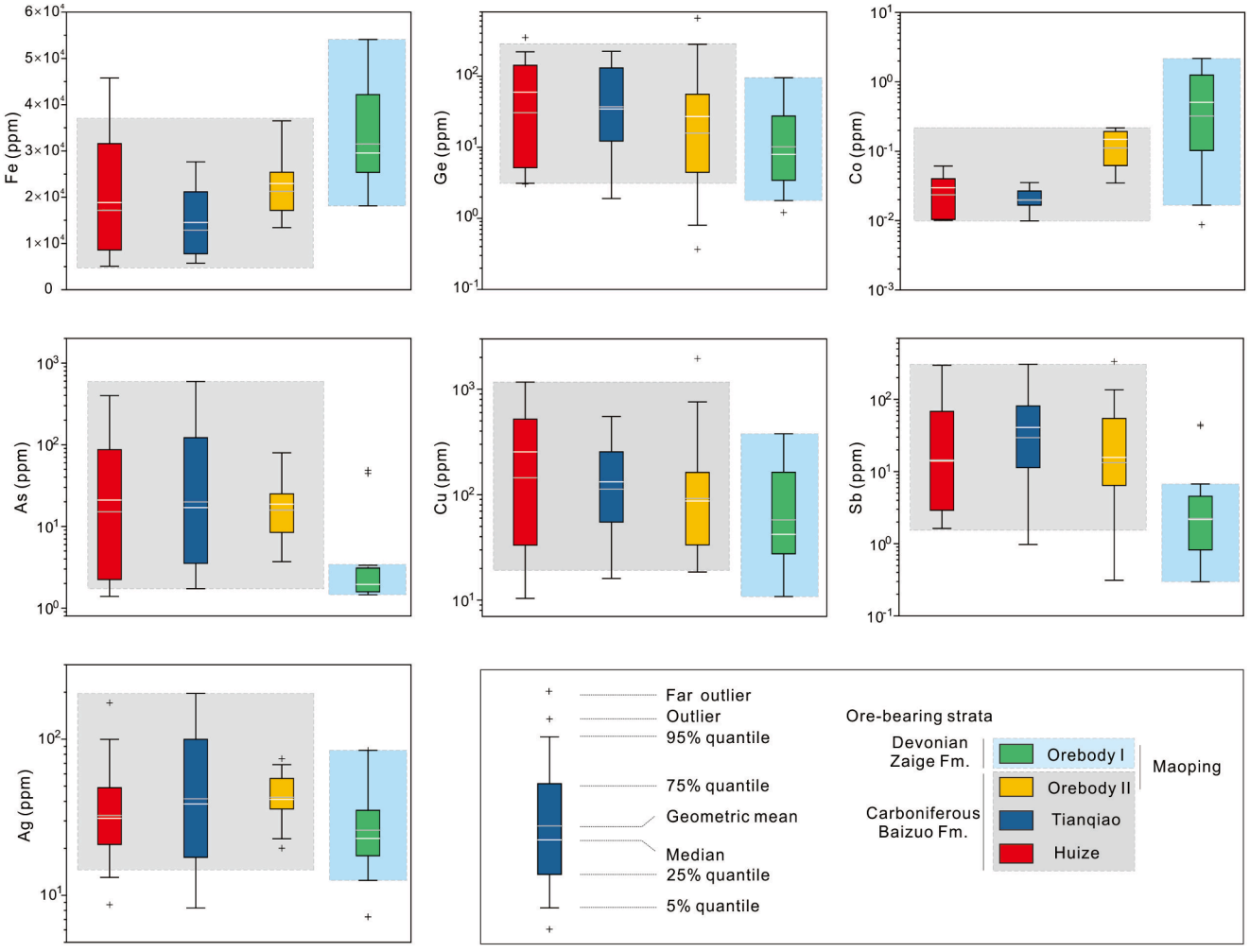

Fig. 10. Box and whisker plots of trace elements in sphalerite hosted in different carbonate rock from different deposits. Plotted analyses including those of sphalerite hosted in the Devonian Zaige Fm. (Orebody I in Maoping). and Carboniferous Fm. (Orebody II in Maoping, Huize from Ye et al. (2011), Tianqiao from our Unpub.). The meaning of symbols in box and whisker plot is the same as Fig. 8.

between two orebodies. This result is further supported by similar trace elements compositions in sphalerite gains selected from same strata. Carbonate-hosted Zn-Pb deposits including Huize and Tiaoqiao, located > 200 km from Maoping, share similar host rock (Carboniferous carbonate rocks) with Orebody II of the Maoping deposit. The similar distribution of Fe, Co, Cu, Ge, As, Ag and Sb in sphalerite have been observed between these deposits and Orebody II of Maoping (Fig. 10). Other elements such as In, Sn and Tl display extremely low contents (the highest geometric mean < 5.6 ppm; Table 2). Therefore, we consider that host rock composition during water-host rock interaction may be the principal control of the variation of these elements (Fe, Co, Cu, Ge, As, Ag, Sb, etc.) in sphalerite from Orebody I and II. But the potential effect of the amount of data cannot be completely excluded.

6.4. Ore genesis

The spatial association between sulfide orebodies and the Emeishan basalt has led many authors to propose a genetic connection between the sulfide mineralization and the magmatism related to the Emeishan mantle plume. They argue that the Maoping deposit is a distal magmatic-hydrothermal deposit (Liu, 1995; Wang, 2001; Xu et al., 2014). However, Rb-Sr dating sphalerite shows that the Maoping deposit occurred in 202.5 ± 8.5 Ma (Yang et al., 2019), younger than the eruption of the Emeishan mantle plume ~ 50 Ma. Moreover, none of intrusions associated with the Zn-Pb mineralization in Maoping have been discovered (Wei et al., 2015; Yang et al., 2019). George et al. (2015) found that the magmatically-driven hydrothermal systems (i.e., Epithermal, VMS and skarn deposits) is relatively enriched in Bi (commonly > 10 ppm, up to 1.0 wt%) and Se (commonly > 10 ppm, up to 1000 ppm), but both Bi and Se in galena from Maoping is normally < 1 ppm. All these evidence could not support a genetic relationship with the magma activities related to the Emeishan mantle plume.

As mentioned in Section 3.3, the sulfide orebodies in the Maoping deposit occur as steeply pipe shape and hosted within the Devonian and Carboniferous carbonate rocks. The hydrothermal alteration is relatively simple and mainly consists of dolomitization, host rock dissolution and brecciation. Ore minerals mainly include sphalerite, galena, dolomite, calcite and minor pyrite and quartz. Sulfur isotope indicates that reduced sulfur was likely derived from the marine sulfate in the ore hosting strata by thermal-chemical reduction (e.g., Yang et al., 2019). Microthermometric data suggest that the ore-forming fluid in the Maoping deposit is characterized by medium–low temperatures (170–247 °C) and moderate-low salinities (4.1–20.5 wt% NaCl equiv.) (Han et al., 2007; Ji, 2019). All these geological and geochemical features of the Maoping deposit compare to those of the MVT deposits (Leach et al., 2005; Ye et al., 2011). This interpretation further supported by trace elements in sphalerite.

Early studies considered that trace element composition of natural sphalerite can be employed to fingerprint different genetic types of Zn-Pb deposits (Zhang, 1987; Cook et al., 2009; Ye et al., 2011, 2016;

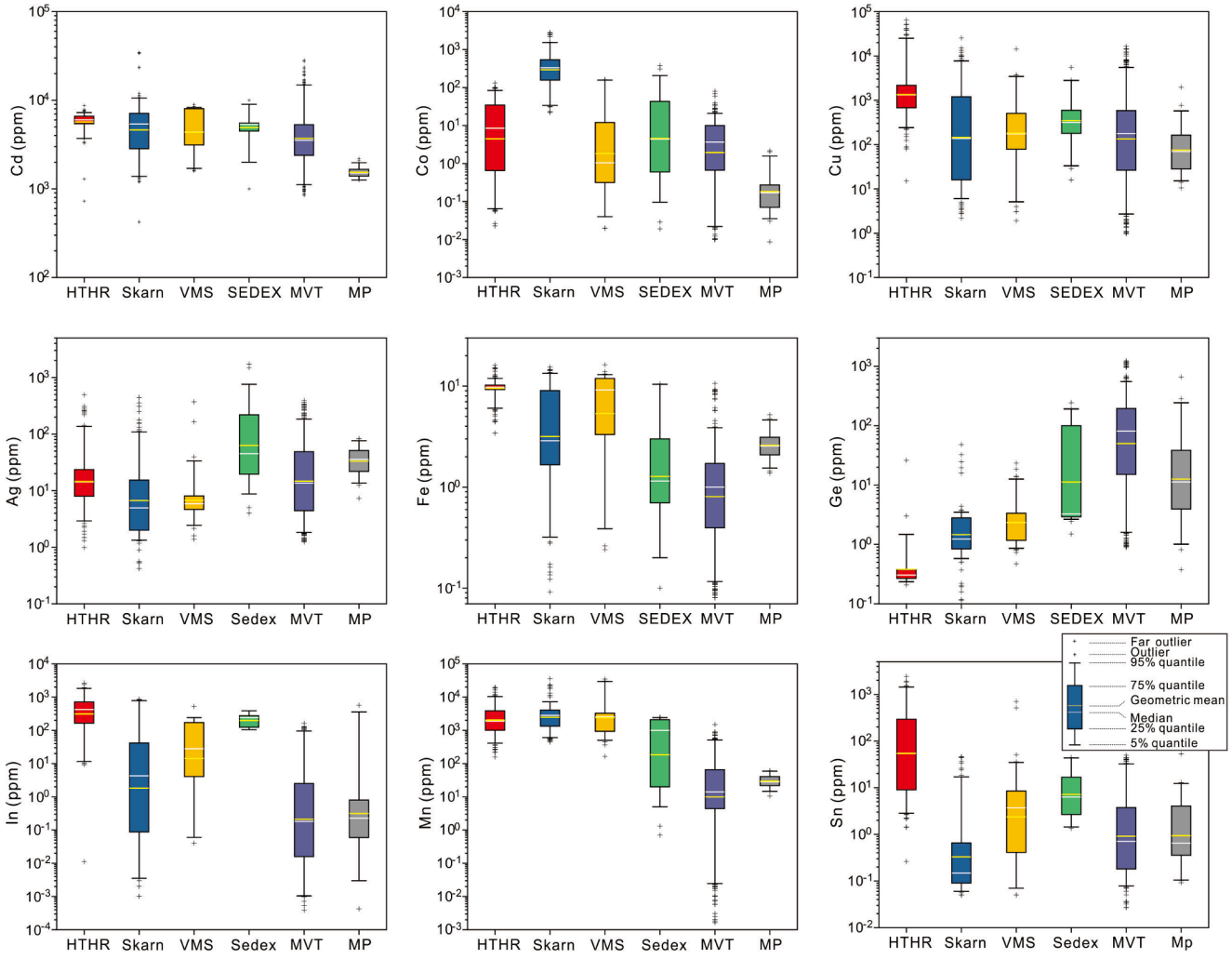

Fig. 11. In-situ minor/trace elements in sphalerite from the Maopin deposit compared with High-temperature hydrothermal (HTHR), Skarn, VMS, SEDEX and MVT deposits. Data from Kelley et al. (2004), Cook et al. (2009), Ye et al. (2011), Wei et al. (2018), Bauer et al. (2018), Knörsch et al. (2019) and Hu et al. (2020).

Frenzel et al., 2016). Many elements in sphalerite, including Fe, Mn, Co, Cd, In, Sn, Sb, Cu, Ge and Ag, have been used to discriminate the genetic type of Zn-Pb deposit. For example, Ye et al. (2012) proposed several binary diagrams to discriminate MVT, VMS, magmatic-hydrothermal and skarn deposits. These discrimination diagrams are useful in identifying the sphalerite with unknown origin. For the Maoping deposit, trace element in sphalerite is characterized by depletions of In, Co and Mn, which is lower than those in the high-*T* magmatic-hydrothermal, VMS and SEDEX (commonly In > 100 ppm and Mn > 1000 ppm; Cook et al., 2009; Ye et al., 2011; Frenzel et al., 2016; Fig. 11) and skarn deposits (commonly Co > 200 ppm and Mn > 1000 ppm; Cook et al., 2009; Ye et al., 2011; Frenzel et al., 2016; Fig. 11). While the measured sphalerite is relatively enriched in Cd and Ge that are analogous to those of MVT deposits from the USA, China and Germany (Ye et al., 2011; Frenzel et al., 2016; Bonnet et al., 2016; Knorsch et al., 2020; Hu et al., 2020; Fig. 11). A similar result has been shown in Fig. 12 where the samples of sphalerite were plotted into the area of MVT deposits. Overall, the compositions of trace element in sulfide from the Maoping deposit is

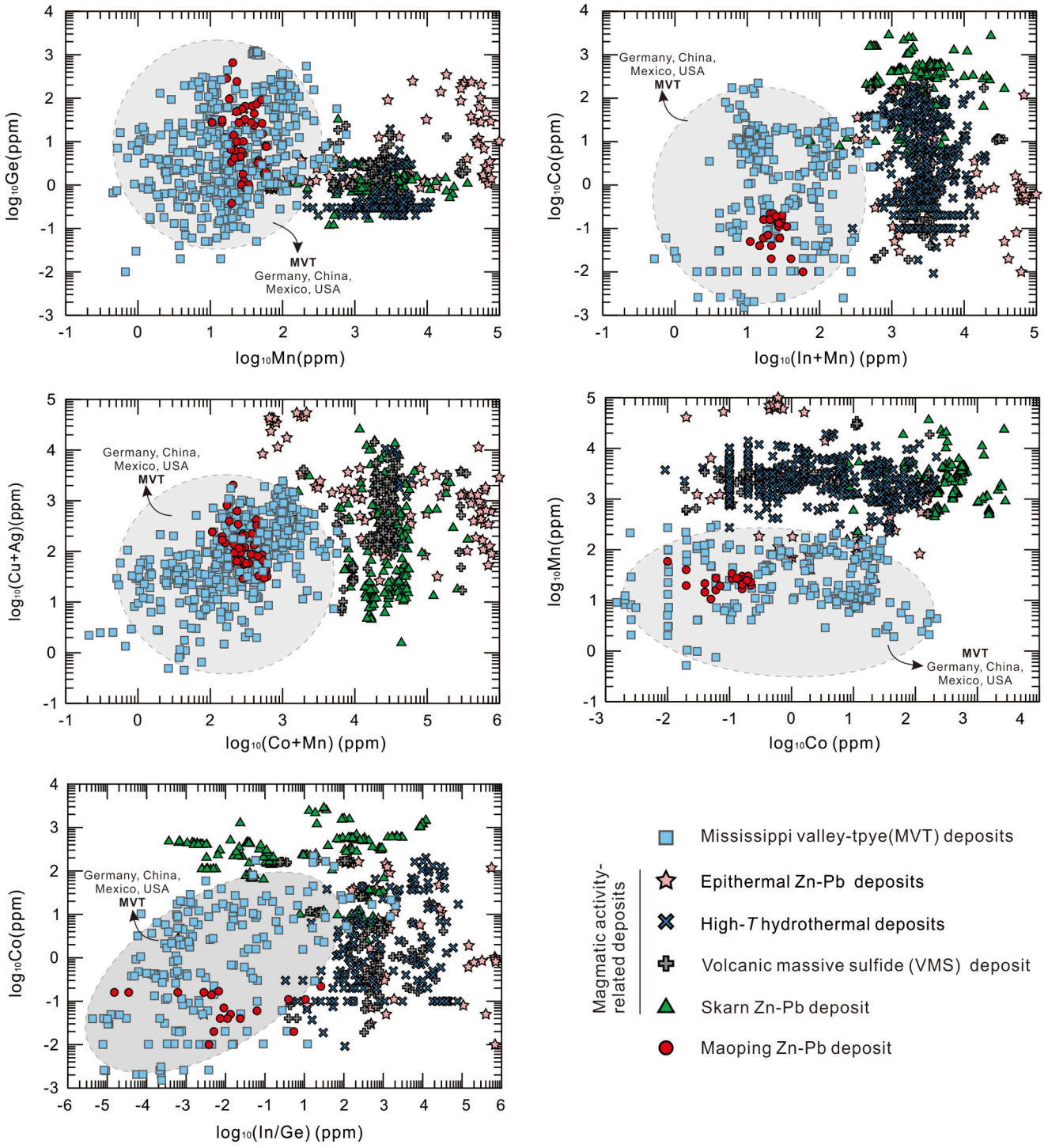

Fig. 12. Binary plots of Mn *vs.* Ge (A), In + Mn *vs.* Co (B), Co + Mn *vs.* Cu + Ag (C), Co *vs.* Mn (D) and In/Ge *vs.* Co (E) in sphalerite from the Maoping Zn-Pb deposit and MVT, VMS, epithermal, skarn, High-*T* hydrothermal Zn-Pb deposits in China, NE Europe, Canada, Germany, USA, Mexico and Japan. Data from Cook et al. (2009), Ye et al. (2011), Wei et al. (2018),Bauer et al. (2018), Knörsch et al. (2019) and Hu et al. (2020).

significantly different from that of the magmatically-driven hydrothermal systems (i.e., Epithermal, VMS and skarn deposits) but consistent with that of the MVT deposits. Overall, newly obtained trace elements in sphalerite and galena together with the geological and geochemical features of the deposit suggest the Maoping deposit should be described as an MVT Zn-Pb deposit.

7. Conclusions and implications

(1) Sphalerite geothermometer studies suggest the ore-forming fluid is a median-low temperature (<250 °C) hydrothermal system accompanied with low fO_2, consisting with previous estimations of dolomite formation.
(2) Several trace elements partitioning between sphalerite and galena in the median-low temperature (<250 °C) hydrothermal system was identified. Sphalerite preferentially incorporates Mn, Cd, Fe, Ge, Cu, In and Sn. Galena is, however, a better host for As, Ag, Sb, Tl and Bi than sphalerite. Although Cd, Co, Ge and Cu tend to concentrate in sphalerite, galena still can host a small amount of these elements.
(3) The variation of trace and minor elements in sphalerite in two orebodies may be mainly controlled by host rock composition, but the contribution from physicochemical conditions (e.g., temperature, fO_2, and pH) and/or source reservoirs of metal elements cannot be ruled out..
(4) Sphalerite from the Maoping deposit is characterized by high Cd, Ge, and low Mn, Fe, Co and Sn, which is similar to that of typical MVT deposit, and different with that of the magmatically-driven hydrothermal systems (i.e., Epithermal, VMS and skarn deposits), suggesting the Maoping deposit belongs to a MVT deposit.

Declaration of Competing Interest

The authors declare that they have no known competing financial interests or personal relationships that could have appeared to influence the work reported in this paper.

Acknowledgments

This research project was co-funded by the National Natural Science Foundation of China (41673056 and U1812402), the Key Program of Guizhou Natural Science Foundation (Qiankehejichu[2017]1421), the State Key Program of National Natural Science Foundation of China (41430315), and National Key R&D Program of China (2017YFC0602502). We are grateful to Dr. Max Frenzel, and Associate Editor Alla Dolgopolova for their insightful comments on our manuscript.

Appendix A. Supplementary data

Supplementary data to this article can be found online at https://doi.org/10.1016/j.oregeorev.2020.103945.

References

Bao, Z., Li, Q., Wang, C.Y., 2017. Metal source of giant Huize Zn-Pb deposit in SW China: New constraints from in situ Pb isotopic compositions of galena. Ore Geol. Rev. 91, 824–836. https://doi.org/10.1016/j.oregeorev.2017.08.019.

Barton, P.B.J., Bethke, P.M., Roedder, H., 1977. Environments of ore deposition in the Creede mining district. San Juan Mountains. Colorado. III. Progress towards interpretation of the chemistry of the ore-forming fluid for the OH vein. Econ. Geol. 12, 1–24.

Bauer, M.E., Burisch, M., Ostendorf, J., Krause, J., Frenzel, M., Seifert, T., Gutzmer, J., 2019. Trace element geochemistry of sphalerite in contrasting hydrothermal fluid systems of the Freiberg district, Germany: insights from LA-ICP-MS analysis, near-infrared light microthermometry of sphalerite-hosted fluid inclusions, and sulfur isotope geochemistry. Miner. Deposita. 54 (2), 237–262. https://doi.org/10.1007/s00126-018-0850-0.

Bernstein, L.R., 1985. Germanium geochemistry and mineralogy. Geochim. Cosmochim. Acta 49 (11), 2409–2422. https://doi.org/10.1016/0016-7037(85)90241-8.

Bethke, P.M., Borton Jr., P.B., 1971. Distribution of some minor elements between coexisting sulphide minerals. Econ. Geol. 66, 140–163.

Bonnet, J., Mosser-Ruck, R., Caumon, M.C., Rouer, O., Andre-Mayer, A.S., Cauzid, J., Peiffery, C., 2016. Trace Element Distribution (Cu, Ga, Ge, Cd, and Fe) in Sphalerite from the Tennessee MVT Deposits, USA, By Combined EMPA, LA-ICP-MS, Raman Spectroscopy, and Crystallography. Can. Mineral. 54 (5), 1261–1284.

Cook, N.J., Ciobanu, C.L., Pring, A., Skinner, W., Shimizu, M., Danyushevsky, L., Saini-Eidukat, B., Melcher, F., 2009. Trace and minor elements in sphalerite: a LA-ICPMS study. Geochim. Cosmochim. Acta 73 (16), 4761–4791. https://doi.org/10.1016/j.gca.2009.05.045.

Cook, N.J., Sundblad, K., Valkama, M., Nygård, R., Ciobanu, C.L., Danyushevsky, L., 2011. Indium mineralisation in A-type granites in southeastern Finland: insights into mineralogy and partitioning between coexisting minerals. Chem. Geol. 284 (1-2), 62–73. https://doi.org/10.1016/j.chemgeo.2011.02.006.

Cugerone, A., Cenki-Tok, B., Chauvet, A., Le Goff, E., Bailly, L., Alard, O., Allard, M., 2018. Relationships between the occurrence of accessory Ge-minerals and sphalerite in Variscan Pb-Zn deposits of the Bossost anticlinorium, French Pyrenean Axial Zone: Chemistry, microstructures and ore-deposit setting. Ore Geol. Rev. 95, 1–19. https://doi.org/10.1016/j.oregeorev.2018.02.016.

Danyushevsky, L., Robinson, P., Gilbert, S., Norman, M., Large, R., McGoldrick, P., Shelley, M., 2011. Routine quantitative multi-element analysis of sulphide minerals by laser ablation ICP-MS: Standard development and consideration of matrix effects. Geochem. Explor. Environ. Anal. 11 (1), 51–60. https://doi.org/10.1144/1467-7873/09-244.

Doe, B.R., Delevaux, M.H., 1972. Source of lead in southeast Missouri galena ores. Econ. Geol., 67: 409–425.

Frenzel, M., Hirsch, T., Gutzmer, J., 2016. Gallium, germanium, indium, and other trace and minor elements in sphalerite as a function of deposit type — a meta-analysis. Ore Geol. Rev. 76, 52–78. https://doi.org/10.1016/j.oregeorev.2015.12.017.

Gagnevin, D., Menuge, J.F., Kronz, A., Barrie, C., Boyce, A.J., 2014. Minor elements in layered sphalerite as a record of fluid origin, mixing, and crystallization in the navan Zn-Pb ore deposit, Ireland. Econ. Geol. 109 (6), 1513–1528. https://doi.org/10.2113/econgeo.109.6.1513.

George, L., Cook, N.J., Ciobanu, C.L., Wade, B.P., 2015. Trace and minor elements in galena: a reconnaissance LA-ICP-MS study. Am. Mineral. 100 (2-3), 548–569. https://doi.org/10.2138/am-2015-4862.

George, L.L., Cook, N.J., Ciobanu, C.L., 2016. Partitioning of trace elements in co-crystallized sphalerite–galena–chalcopyrite hydrothermal ores. Ore Geol. Rev. 77, 97–116. https://doi.org/10.1016/j.oregeorev.2016.02.009.

Guo, X., 2011. Mineralization and metallogenic pattern of lead-zinc deposits in Northeast Yunnan. Doctoral Dissertation, China University of Geosciences, 1–167 (in Chinese with English abstract).

Han, R.S., Zou, H.J., Hu, B., Hu, Y.Z., Xue, C.D., 2007. Features of fluid inclusions and sources of ore-forming fluid in the Maoping carbonate-hosted Zn-Pb-(Ag-Ge) deposit, Yunan, China. Acta Petrol. Sinica 23 (9), 2109–2118.

Han, R.S., Hu, Y.Z., Wang, X.K., Hou, B.H., Huang, Z.L., Chen, J., Wang, F., Wu, P., Li, B., Wang, H.J., Dong, Y., Lei, L., 2012. Mineraliztion model of rich Ge-Ag-bearing Zn-Pb polymetallic deposit concentrated district in Northeastern Yunnan, China. Acta Geol. Sinica 86 (2), 280–294 (in Chinese with English abstract).

He, B., Xu, Y.-G., Huang, X.-L., Luo, Z.-Y., Shi, Y.-R., Yang, Q.-J., Yu, S.-Y., 2007. Age and duration of the Emeishan flood volcanism, SW China: Geochemistry and SHRIMP zircon U–Pb dating of silicic ignimbrites, post-volcanic Xuanwei Formation and clay tuff at the Chaotian section. Earth Planet. Sci. Lett. 255 (3-4), 306–323. https://doi.org/10.1016/j.epsl.2006.12.021.

He, Y.F., 2019. Geochemistry and genesis of the Maoping superlarge lead-zinc deposit in northeastern Yunnan. Ph.D. Dissertation. Institute of Geochemistry, Chinese Academy of Sciences, Guiyang, 1–123 (in Chinese with English abstract).

Höll, R., Kling, M., Schroll, E., 2007. Metallogenesis of germanium—a review. Ore Geol. Rev. 30 (3-4), 145–180. https://doi.org/10.1016/j.oregeorev.2005.07.034.

Hu, R., Fu, S., Huang, Y., Zhou, M.-F., Fu, S., Zhao, C., Wang, Y., Bi, X., Xiao, J., 2017. The giant South China Mesozoic low-temperature metallogenic domain: reviews and a new geodynamic model. J. Asian Earth Sci. 137, 9–34. https://doi.org/10.1016/j.jseaes.2016.10.016.

Hu, Y.S., Ye, L., Huang, Z.L., Li, Z.L., Wei, C., Danyushevsky, L., 2019. Distribution and existing forms of trace elements from Maoliping Pb-Zn deposit in northeastern Yunan, China: a LA-ICP-MS study. Acta Petrol. Sinica 35 (11), 3477–3492 (in Chinese with English abstract).

Hu, Y.S., Ye, L., Wei, C., Li, Z.L., Huang, Z.L., Wang, H.Y., 2020. Trace elements in sphalerite from the Dadongla Zn-Pb deposit, Western Hunan–Eastern Guizhou Zn-Pb metallogenic belt, South China. Acta Geol. Sinica (English Edition) 94 (6), 2152–2164.

Huang, Z.L., Chen, J., Han, R.S., Li, W.B., Liu, C.Q., Zhang, Z.L., Ma, D.Y., Gao, D.R., Yang, H.L., 2004. Geochemistry and ore-formation of the Huize Giant Lead-zinc Deposit, Yunnan Province. In: China: Discussion on the Relationship between the Emeishan Flood Basalts and Lead-zinc Mineralization. Geological Publishing House, Beijing, pp. 1–214 (in Chinese).

Hutchison, M.N., Scott, S.D., 1983. Experimental calibration of the sphalerite cosmobarometer. Geochim. Cosmochim. Acta 47 (1), 101–108. https://doi.org/10.1016/0016-7037(83)90094-7.

Ji, P.L., 2019. Geochemical characteristics and ore-controlling factors of Maoping Pb-Zn deposit in Yiliang County, Yunnan Province. Master Degree Thesis. Chengdu University of Technology, 1–85 (in Chinese with English abstract).

Kelley, K.D., Leach, D.L., Johnson, C.A., Clark, J.L., Fayek, M., Slack, J.F., Anderson, V. M., Ayuso, R.A., Ridley, W.I., 2004. Textural, compositional, and sulfur isotope

variations of sulfide minerals in the red dog Zn-Pb-Ag deposits, Brooks Range, Alaska: implications for ore formation. Econ. Geol. 99 (7), 1509–1532. https://doi.org/10.2113/gsecongeo.99.7.1509.

Leach, D.L., Sangster, D., Kelley, K.D., Large, R.R., Garven, G., Allen, C., Gutzmer, J., Walters, S., 2005. Sediment-hosted lead-zinc deposits: a global perspective. Economic Geology 100th Anniversary p. 561–607.

Knorsch, M., Nadoll, P., Klemd, R., 2020. Trace elements and textures of hydrothermal sphalerite and pyrite in Upper Permian (Zechstein) carbonates of the North German Basin. J. Geochem. Explor. 209 https://doi.org/10.1016/j.gexplo.2019.106416.

Li, W., Huang, Z., Yin, M., 2007. Dating of the giant huize Zn-Pb Ore field of Yunnan Province, Southwest China: constraints from the Sm-Nd system in hydrothermal calcite. Resour. Geol. 57 (1), 90–97. https://doi.org/10.1111/j.1751-3928.2006.00007.x.

Lin, Z.Y., Wang, D.H., Zhang, C.Q., 2010. Rb-Sr isotopic age of sphalerite from the Paoma lead-zinc deposit in Sichuan Province and its implications. Geol. China 37, 488–1196 (in Chinese with English abstract).

Liu, H.C., 1995. Emeishan basalt and Pb-Zn metallogenesis. Geol. Prospect. 31 (4), 1–6 (in Chinese with English abstract).

Liu, H.C., Lin, W.D., 1999. Regularity Research of Pb-Zn-Ag Ore Deposits in Northeast Yunnan, China. Yunnan University Press, Kunming, pp. 1–468 (in Chinese).

Longerich, H.P., Jackson, S.E., Gunther, D., 1996. Laser ablation inductively coupled plasma mass spectrometric transient signal data acquisition and analyte concentration calculation. J. Anal. At. Spectrom. 11, 899–904.

Möller, P., 1987. Correlation of homogenization temperatures of accessory minerals from sphalerite-bearing deposits and Ga/Ge model temperatures. Chem. Geol. 61 (1-4), 153–159. https://doi.org/10.1016/0009-2541(87)90035-0.

Oftedahl, I., 1940. Untersuchungen über die Nebenbestandteile von Erzmineralien norwegischer zinkblendführender Vorkommen. Skrift Norsk Vidensk Akad Oslo. Math. Naturv. Kl. 8, 1–103.

Pattrick, R.A.D., Dorling, M., Polya, D.A., 1993. TEM study of indium- and copper-bearing growth-banded sphalerite. Can. Mineral. 31, 105–117.

Paton, C., Hellstrom, J., Paul, B., Woodhead, J., Hergt, J., 2011. Iolite: Freeware for the visualisation and processing of mass spectrometric data. J. Anal. At. Spectrom. 26 (12), 2508. https://doi.org/10.1039/c1ja10172b.

Scott, S.D., 1983. Chemical behavior of sphalerite and arsenopyrite in hydrothermal and metamorphic environments. Mineral. Mag. 47, 427–435.

Scott, S.D., Barnes, H.L., 1971. Sphalerite geothermometry and geobarometry. Economic Geology, 66, 653–669.

Wei, C., Ye, L., Huang, Z.L., Hu, Y.S., Yan, Z.F., n.d.. Fluid mixing forms carbonate-hosted Nayongzhi Zn-Pb deposit, South China: Evidence from geology, In situ S and Pb isotopes and fluid inclusion. Economic Geology. Submitted for publication.

Xiang, Z.-Z., Zhou, J.-X., Luo, K., 2020. New insights into the multi-layer metallogenesis of carbonated-hosted epigenetic Pb-Zn deposits: a case study of the Maoping Pb-Zn deposit, South China. Ore Geol. Rev. 122, 103538. https://doi.org/10.1016/j.oregeorev.2020.103538.

Wang, C.W., Li, Y., Luo, H.Y., Liu, X.L., 2009. Genesis of maoping Pb-Zn deposit in Yunnan Province. J. Kunm. Univ. Sci. Technol. (Sci. Technol.) 34 (1), 7–11 (in Chinese with English abstract).

Wang, D.H., 2001. Basic concept, classification, evolution of Mantle plume and large scale mineralization Probe into southwestern China. Earth Sci. Front. 8 (3), 67–72 (in Chinese with English abstract).

Wang, T., 2019. Study on geology and genesis of the Maoping Lead-zinc deposit, Zhaotong, Yunnan, China. Master Degree Thesis. Chengdu University of Technology, 1–73 (in Chinese with English abstract).

Watling, R.J., Herbert, H.K., Abell, I.D., 1995. The application of laser ablation-inductively coupled plasma-mass spectrometry (LA-ICP-MS) to the analysis of selected sulphide minerals. Chem. Geol. 124 (1-2), 67–81. https://doi.org/10.1016/0009-2541(95)00025-H.

Wei, A., Xue, C., Xiang, K., Li, J., Liao, C., Akhter, Q.J., 2015. The ore-forming process of the Maoping Pb–Zn deposit, northeastern Yunnan, China: constraints from cathodoluminescence (CL) petrography of hydrothermal dolomite. Ore Geol. Rev. 70, 562–577. https://doi.org/10.1016/j.oregeorev.2015.02.007.

Wei, C., Ye, L., Huang, Z.L., Gao, W., Hu, Y.S., Li, Z.L., Zhang, J.W., 2018. Ore Genesis and Geodynamic Setting of Laochang Ag-Pb-Zn-Cu Deposit, Southern Sanjiang Tethys Metallogenic Belt, China: constraints from Whole Rock Geochemistry, Trace Elements in Sphalerite, Zircon U-Pb Dating and Pb Isotopes. Minerals, 8(11): 516.

Wei, C., Ye, L., Hu, Y., Danyushevskiy, L., Li, Z., Huang, Z., 2019. Distribution and occurrence of Ge and related trace elements in sphalerite from the Lehong carbonate-hosted Zn-Pb deposit, northeastern Yunnan, China: insights from SEM and LA-ICP-MS studies. Ore Geol. Rev. 115, 103175. https://doi.org/10.1016/j.oregeorev.2019.103175.

Xu, Y., Huang, Z.L., Zhu, D., Luo, T.Y., 2014. Origin of hydrothermal deposits related to theEmeishan magmatism. Ore Geol. Rev. 63, 1–8.

Yang, Q., Liu, W., Zhang, J., Wang, J., Zhang, X., 2019. Formation of Pb–Zn deposits in the Sichuan–Yunnan–Guizhou triangle linked to the Youjiang foreland basin: evidence from Rb–Sr age and in situ sulfur isotope analysis of the Maoping Pb–Zn deposit in northeastern Yunnan Province, southeast China. Ore Geol. Rev. 107, 780–800. https://doi.org/10.1016/j.oregeorev.2019.03.022.

Ye, L., Cook, N.J., Ciobanu, C.L., Yuping, L., Qian, Z., Tiegeng, L., Wei, G., Yulong, Y., Danyushevskiy, L., 2011. Trace and minor elements in sphalerite from base metal deposits in South China: a LA-ICPMS study. Ore Geol. Rev. 39 (4), 188–217. https://doi.org/10.1016/j.oregeorev.2011.03.001.

Ye, L., Gao, W., Yang, Y.L., Liu, T.G., Peng, S.S., 2012. Trace elements in sphalerite in Laochang Pb-Zn polymetallic deposit, Lancang, Yunnan Province. Acta Petrol. Sinica 28 (5), 1362–1372 (in Chinese with English abstract).

Ye, L., Li, Z.L., Hu, Y.S., Huang, Z.L., Zhou, Z.J., Fan, H.F., Danyushevskiy, L., 2016. Trace element in sulfide from Tianbaoshan Pb-Zn deposit, Sichuan province, China: A LA-ICPMS study. Acta Petrol. Sinica 32 (11), 3377–3393 (in Chinese with English abstract).

Zaw, K., Peters, S.G., Cromie, P., Burrett, C., Hou, Z., 2007. Nature, diversity of deposit types and metallogenic relations of South China. Ore Geol. Rev. 31 (1-4), 3–47. https://doi.org/10.1016/j.oregeorev.2005.10.006.

Zhang, C., Wu, Y., Hou, L., Mao, J., 2015. Geodynamic setting of mineralization of Mississippi Valley-type deposits in world-class Sichuan–Yunnan–Guizhou Zn–Pb triangle, southwest China: implications from age-dating studies in the past decade and the Sm–Nd age of Jinshachang deposit. J. Asian Earth Sci. 103, 103–114. https://doi.org/10.1016/j.jseaes.2014.08.013.

Qian, Z., 1987. Trace elements in galena and sphalerite and their geochemical significance in distinguishing the genetic types of Pb-Zn ore deposits. Chin. J. of Geochem. 6 (2), 177–190. https://doi.org/10.1007/BF02872218.

Zheng, M.H., Wang, X.C., 1991. Genesis of the Daliangzi Pb-Zn deposit in Sichuan, China. Econ. Geol. 86, 831–846.

Zhou, G.M., Li, B.L., 2005. Geological characteristics and original discussion on genesis of the lead-zinc deposit of Maoping in Yunnan Province. West-China Explor. Eng. 106 (3), 75–77 (in Chinese with English abstract).

Zhou, J., Huang, Z., Yan, Z., 2013a. The origin of the Maozu carbonate-hosted Pb–Zn deposit, southwest China: constrained by C–O–S–Pb isotopic compositions and Sm–Nd isotopic age. J. Asian Earth Sci. 73, 39–47. https://doi.org/10.1016/j.jseaes.2013.04.031.

Zhou, J., Huang, Z., Zhou, M., Li, X., Jin, Z., 2013b. Constraints of C–O–S–Pb isotope compositions and Rb–Sr isotopic age on the origin of the Tianqiao carbonate-hosted Pb–Zn deposit, SW China. Ore Geol. Rev. 53, 77–92. https://doi.org/10.1016/j.oregeorev.2013.01.001.